c.1

ELLIPSOMETRIC INVESTIGATION OF THE MECHANISM OF HOLOGRAM STORAGE IN LITHIUM NIOBATE

by

William K.Y. Wong

B.A.Sc., University of British Columbia, 1971

A THESIS SUBMITTED IN PARTIAL FULFILMENT OF THE REQUIREMENTS FOR THE DEGREE OF MASTER OF APPLIED SCIENCE

in the Department of Electrical Engineering

We accept this thesis as conforming to the required standard

THE UNIVERSITY OF BRITISH COLUMBIA

AUGUST, 1973

In presenting this thesis in partial fulfilment of the requirements for an advanced degree at the University of British Columbia, I agree that the Library shall make it freely available for reference and study. I further agree that permission for extensive copying of this thesis for scholarly purposes may be granted by the Head of my Department or by his representatives. It is understood that copying or publication of this thesis for financial gain shall not be allowed without my written permission.

Department of Electrical Engineering.

The University of British Columbia
Vancouver 8, Canada

Date Sept 5 1973.

ABSTRACT

A computer-controlled ellipsometer was used to obtain data on the birefringence changes induced in lithium niobate crystals by irradiation with an argon-ion laser. The instrument was set to take readings on a rectangular grid of points before and after irradiation. Irradiation was performed with circular and with narrow rectangular light beams. Results are compared with the prediction of the model of Chen in which he postulated the presence of an internal field E_o in the direction of the c-axis of the crystal. According to his theory, electrons, photoexcited from traps by the laser light, drift under the influence of E_o along the c-axis before being retrapped. The resulting space-charge field set between positive ionised centres and trapped electrons gives rise to the observed birefringence changes via the linear electro-optic effect of the crystal. Approximate mathematical models based on Chen's theory are used to solve the problem with narrow rectangular light beams. Results are compared with experiments.

TABLE OF CONTENTS

LIST OF ILLUSTRATIONS

ACKNOWLEDGEMENT

I am most grateful to Dr. L. Young for his helpful suggestion and guidance during the course of this work.

The financial support of this work by the Canadian Defence Research Board (DRB Grant 5501-67) is most gratefully acknowledged.

Grateful acknowledgement for financial support is also given to the National Research Council (scholarship awarded 1972-1973) and the University of British Columbia (fellowship awarded 1971-1972).

I wish to thank Mr. W. Cornish and Mr. M. Thewalt for many helpful suggestions and technical assistance.

Finally I wish to thank Miss Norma Duggan and Miss Betty Cockburn for help in typing the thesis.

I. INTRODUCTION

Modern data processing systems use a hierarchy of storage devices ranging from cores, disks, tapes to semiconductor memories. Mass optical memories[1] are currently under active consideration as a powerful addition to this hierarchy. Various types of optical memories have been proposed and in some cases realized. One particular type is the large scale read-write optical memory based on hologram storage on an erasable medium and compound addressing by pages and within pages. An array of light valves composes the page to be stored. The direction of illumination of the page composer, resulting from deflection of a laser beam, determines the location on the storage medium at which a hologram of the page will be recorded (and the previous record erased). The page composer and sensor array are physically combined with an electrically addressable memory. This type of optical memories seems to be of particular promise as an extension of this hierarchy where large amounts of information ($> 10^8$ bits) must be fairly rapidly accessible ($\sim \mu$sec) on a page by page basis.

This thesis is concerned with studying the mechanism by which information is stored in one of the possible candidates for the storage medium - lithium niobate ($LiNbO_3$). Lithium niobate has many advantages as far as holographic storage is concerned: holographic diffraction efficiency as high as 80% has been achieved in lithium niobate doped with iron[2]; storage times of many days are possible at ordinary room temperature and erasure can be achieved either optically or by heating the crystal to 300°C[3]; the holograms stored can also be 'fixed' thermally so that the patterns are optically non-erasable[4]; no bleaching of the

hologram is required. The mechanism by which information is stored in lithium niobate is via 'optical damage', that is , lithium niobate responds to laser light of the appropriate wavelength with change in the refractive index. Although this effect is detrimental to the operation of this material in electro-optic modulation and second harmonic generation, Chen[6] and others[7] have used this effect to store thick phase holograms in lithium niobate. With these facts in mind, the purpose of the thesis is to investigate the mechanism of holographic storage in lithium niobate by studying the optical damage using a computer-controlled ellipsometer.

Chapter II gives a brief description of the experimental set up, the optical damage procedure and shows how the ellipsometer readings are related to refractive index measurements.

In Chapter III, the patterns of refractive index change due to a circular damaging laser beam is investigated. The results are explained qualitatively using Chen's model. A brief review of the electro-optic effect in lithium niobate is then given. Finally, numerical methods based on King's analysis of optical damage in KTN are used to treat this problem quantitatively and the results compared with experiments.

In Chapter IV, the patterns of refractive index change due to a narrow strip of laser light is investigated. A simplified theory based on Chen's model is solved analytically using Laplace transform method. This method is used since it can easily be modified to solve for any other light distributions. The results are then compared with experiments. Finally, the results of an experiment relating to the proposed internal field are discussed.

The conclusions that can be drawn from the above studies are remarked upon in Chapter V.

II. THE GENERAL EXPERIMENTAL ARRANGEMENT

1. Introduction

The lithium niobate crystal used in the experiments was supplied by Harshaw Chemical Company and its dimensions are 2.0 x 1.5 x 0.3 cm^3. The 2.0 x 1.5 cm^2 faces are polished flat to 1/2 wavelength and parallel within one minute at sodium 'D' light within 1 mm of the edge or better. The optical damage was performed by exposing the crystal to a Coherent Radiation argon-ion laser (maximum output=500mW) for specified periods of time. The power of the laser light was measured by a Jordan optical power wattmeter. The resulting optical damage was then probed by placing the crystal in an automated ellipsometer. Before each experiment, the crystal was heated to 500^{o}C for half an hour and then cooled slowly. This treatment was shown to anneal out any space-charge field resulting from optical damage of the previous experiment. Figure 1 shows the rate of cooling

2. Ellipsometer set up

The Rudolph Thin Film Ellipsometer (type 43603-200E), used in this project, was interfaced to a DEC PDP-8/E computer. Only minor additions were required to the existing interface. Figure 2 shows the basic set up.

Light from a Spectra Physics helium-neon laser (model 133) passed through a green filter which cut down the intensity of the laser light so that this probing beam would not optically damage the crystal. (The crystal could be left exposed to this reduced laser light for several hours without showing any sign of being optically damaged.)

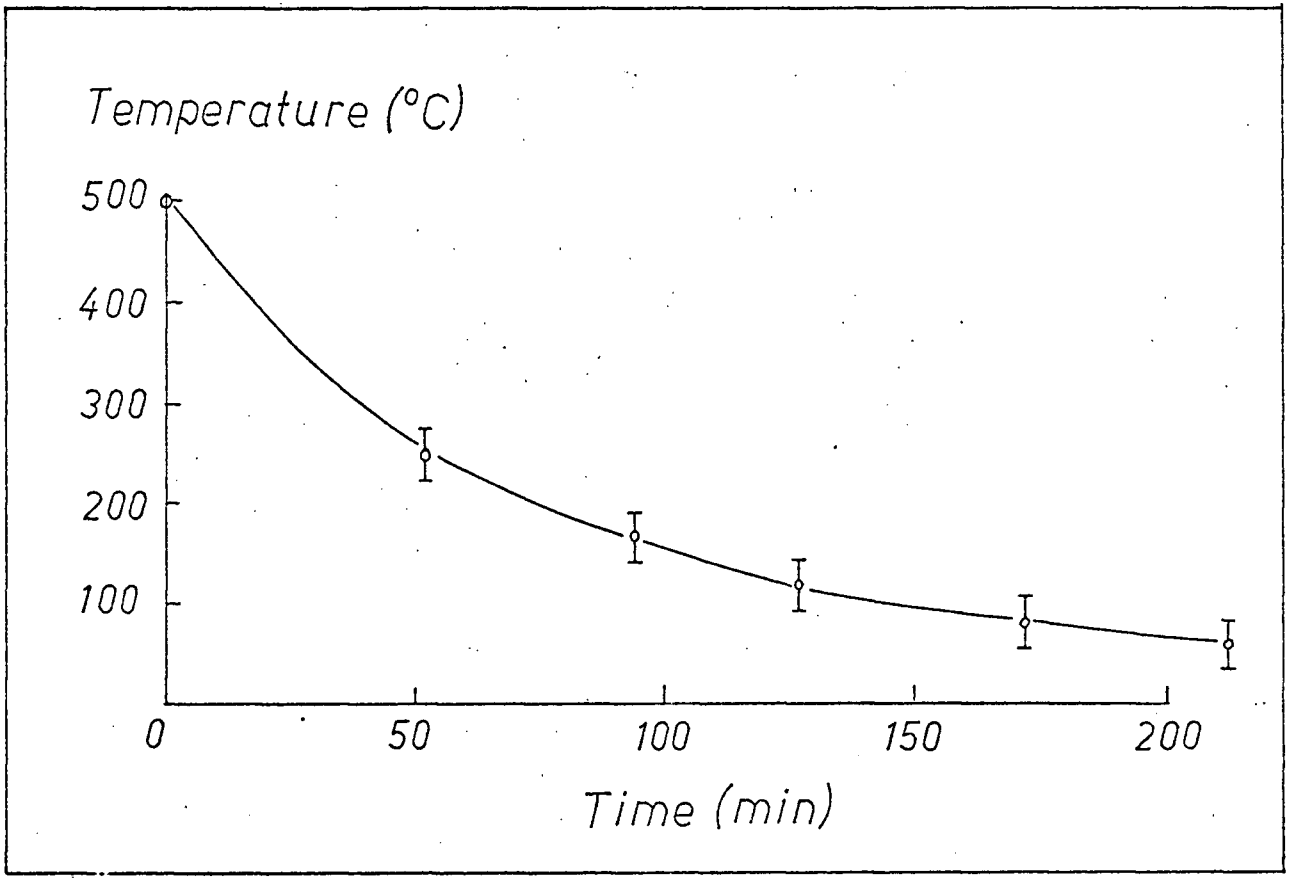

Figure 1: Rate of cooling of crystal after baking to 500°C for 1/2 hour.

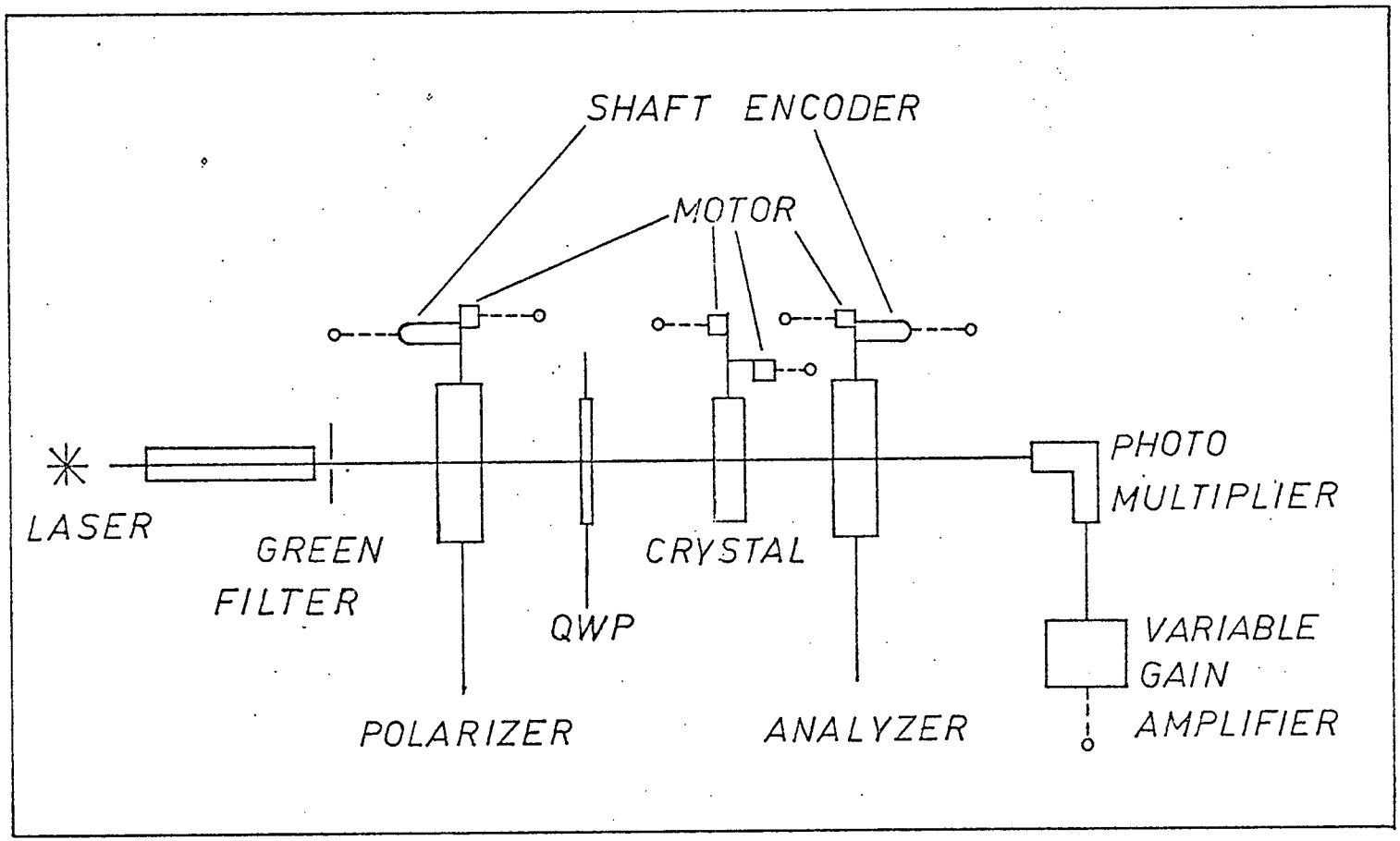

Figure 2: Computer-Ellipsometer interface. Dashed lines indicate connection to the computer interface.

After passing through the polariser, the light was linearly polarised. The quarter-wave plate (QWP) converted the linearly polarised light into elliptically polarised light which was then incident normal to the crystal. Any light emerging from the analyser went into a photo-multiplier and then into a variable gain amplifier interfaced to the computer.

Since the refractive index in lithium niobate is temperature dependent[9], the temperature must be kept constant during measurement. The crystal, held in a sample holder (figure 3), was placed in a plexiglass box with openings at opposite ends of the box to allow the probing laser beam to enter and leave (figure 4). Resistors were used as heating elements and together with a fan, a Yellow Springs Instruments proportional temperature controller and a thermistor as sensing element, the temperature was maintained at $32 \pm 0.05^{\circ}C$. Throughout the whole experiment, the temperature was further monitored by inserting into the box an iron-constantan thermocouple and connecting the output to a strip chart recorder. Stepping motors were mounted to the shaft of the sample holder in such a way that the crystal could be moved in two mutually perpendicular directions normal to the light beam.

3. Optical damage procedure

Before optical damage, the crystal was placed in the set up shown in figure 2. After alignment of the crystal so the the probing laser beam passed normally through it, the ellipsometer was balanced. The balancing procedure will be described in a later section. Stepping motors then moved the crystal to a different position and the

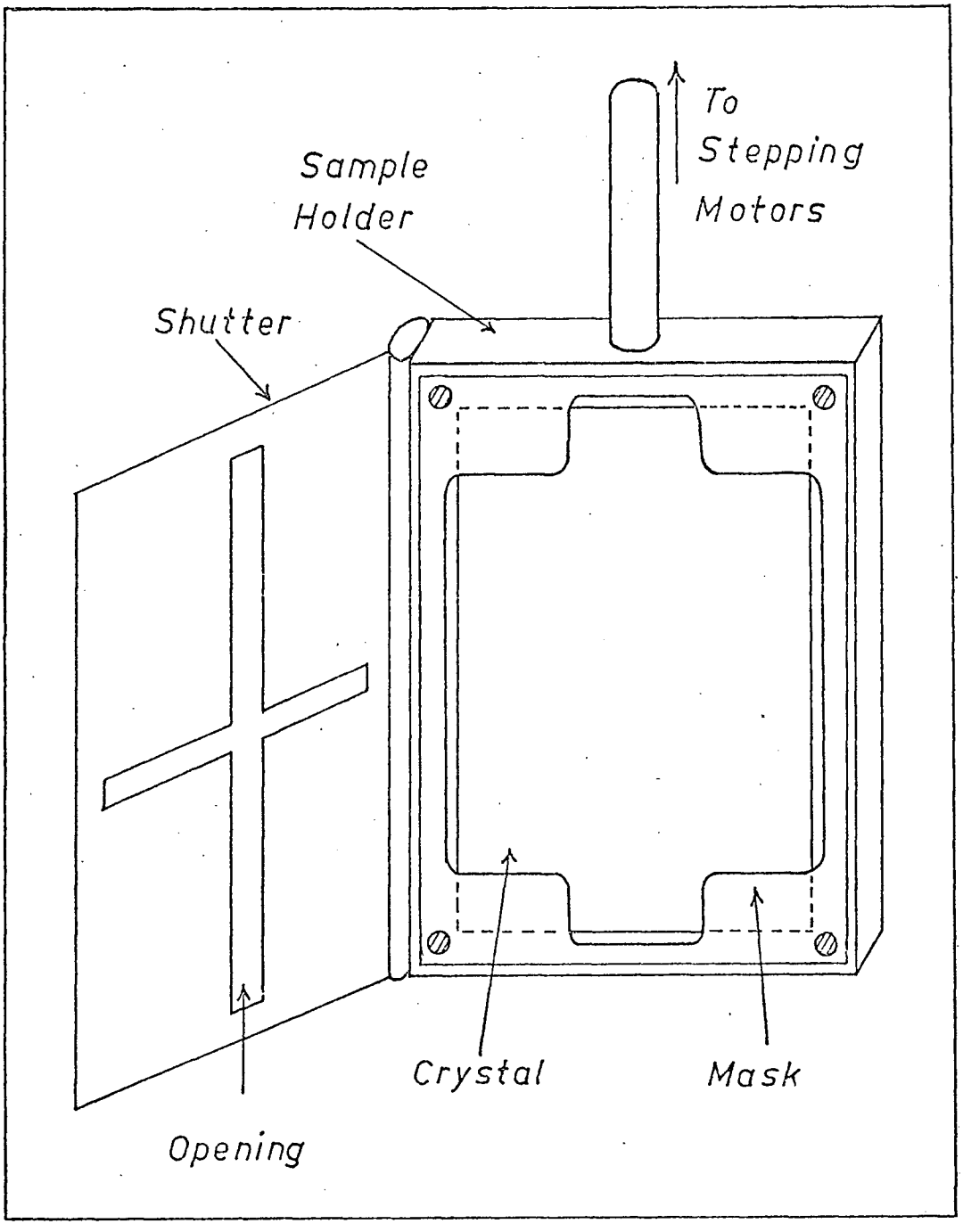

Figure 3: Sample holder for $LiNbO_3$ crystal.

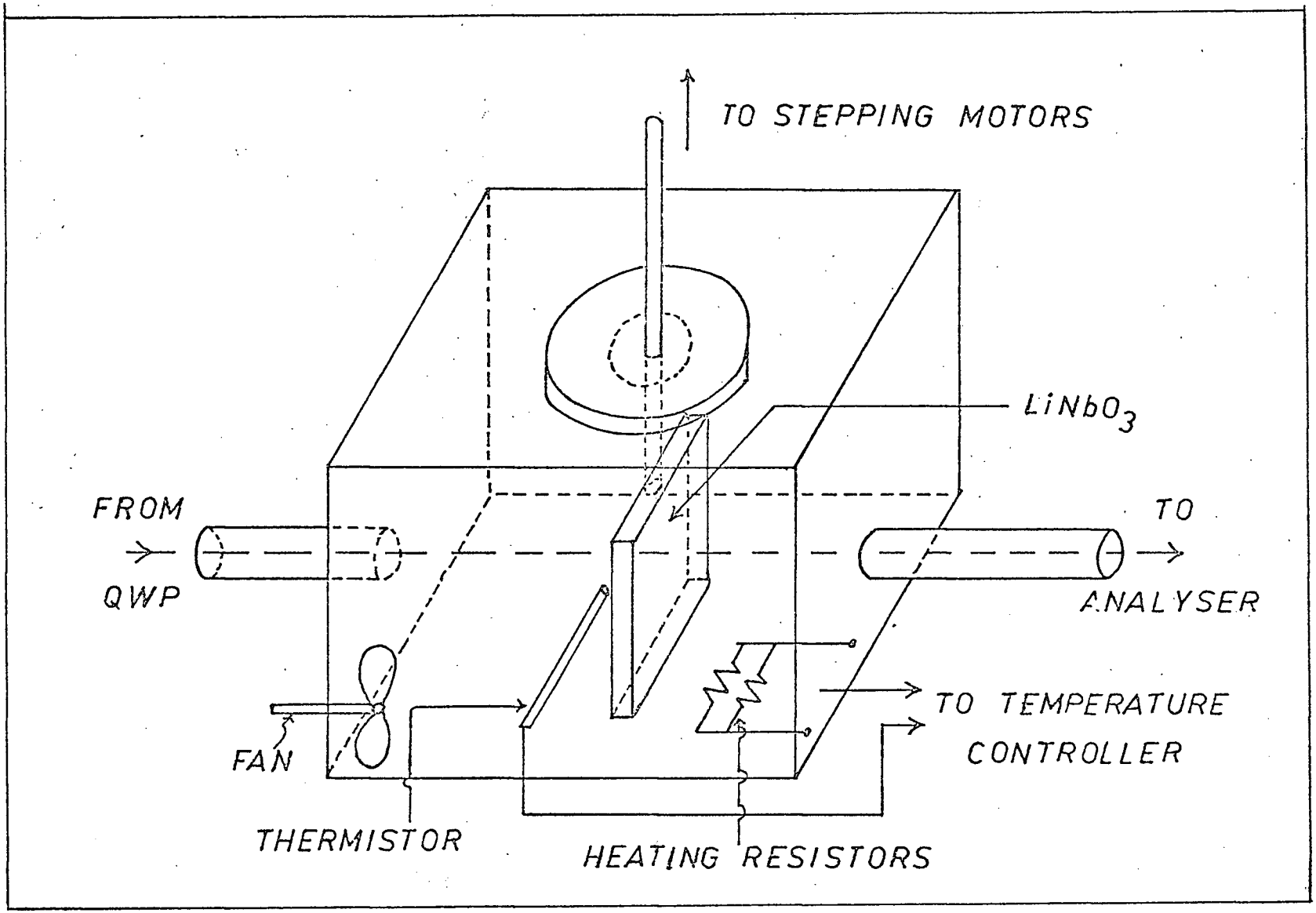

Figure 4: Temperature controlling box.

same procedure was repeated. Continuing in this way, a map of the refractive index variations throughout the crystal was obtained. The data was simultaneously recorded on paper tapes as the ellipsometer was taking reading. The crystal was then removed from the set up and exposed to the argon-ion laser for a specified period of time. It was then replaced in the ellipsometer and the balancing routine repeated. A reference mask attached to the sample holder enabled the crystal to be scanned at the same grid-points before and after the optical damage. In this way a three-dimensional map of the refractive index variations after optical damage was again obtained and the data again recorded on paper tapes. The difference between the two sets of readings gave us a data map of the induced change in the refractive index of the crystal. A program was written for the PDP-8/E to subtract the corresponding numbers on the two paper tapes. The resulting data (on paper tapes) was then copied onto 9-track magnetic tapes in the IBM 360/67 computer using programs provided by the UBC Computing Centre. A perspective view of the induced refractive index change was then plotted using the Computing Centre's program UBC PERSP.

4. Refractive Index Measurements from Ellipsometer Readings

The polariser and analyser are Glan-Thompson prisms mounted in graduated circles which were rotated by stepping motors. Decitrak shaft encoders (TR-511C-CW/D) which were mounted on the analyser and polariser converted the angles to BCD for input to the computer. The stepping motors and shaft encoders were both multiplexed to one device code. The ellipsometer measured P and A, the azimuths of the electric field vector transmitted by the polariser and analyser respectively.

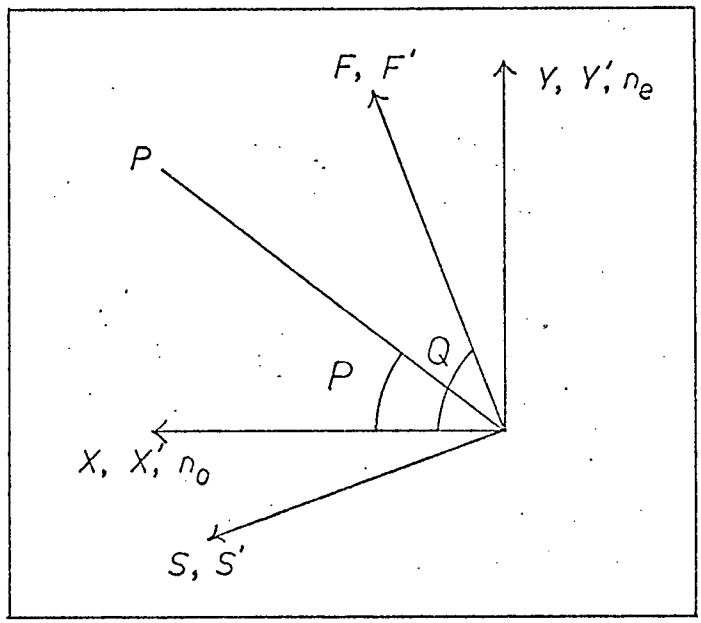

Figure 5: Resolution of light into components as it passes through the ellipsometer.

After passing through the polariser, the light is plane polarised in the direction P (Figure 5). Resolving this into components along the slow and fast axis of the QWP, we get

$$E_F = \cos(Q-P) \qquad E_S = \sin(Q-P) \tag{1}$$

where Q is the azimuth of the fast axis of the QWP. After passing through the QWP. the slow axis component of light is delayed by δ relative to the fast axis (δ is the retardation of the QWP) and assuming no attenuation due to the QWP we have

$$E_F' = E_F \qquad E_S' = E_S \exp -j\delta \tag{2}$$

Resolving this into components along the X and Y axis (n_e and n_o axis of the $LiNbO_3$) we then get

$$E_X = E_F' \cos Q + E_S' \sin Q$$
$$E_Y = E_F' \sin Q - E_S' \cos Q \tag{3}$$

$LiNbO_3$ is a negative uniaxial crystal, that is, $n_o > n_e$ and hence after passing through the crystal, E_X is delayed by ϕ relative to E_Y

$$E_X' = E_X \exp -j\phi \qquad E_Y' = E_Y \tag{4}$$

To be extinguished by the analyser, the light must be plane polarised, or stating it in another way

$$(\text{phase of } E_X) - \phi = (\text{phase of } E_Y) \tag{5}$$

Substituting (1) and (2) into (3), we have

$$E_X = \cos (Q-P) \cos Q + \sin (Q-P) \sin Q \exp -j\delta$$
$$E_Y = \cos (Q-P) \sin Q - \sin (Q-P) \cos Q \exp -j\delta$$

or
$$E_X = C_1 + C_2 \exp -j\delta$$
$$E_Y = C_3 + C_4 \exp -j\delta \tag{6}$$

where $C_1 = \cos (Q-P) \cos Q \qquad C_2 = \sin (Q-P) \sin Q$

$C_3 = \cos (Q-P) \sin Q \qquad C_4 = -\sin (Q-P) \cos Q$

Now $\exp -j\delta = \cos\delta - j \sin\delta$

Hence equation (6) can be written

$$E_X = (C_1 + C_2 \cos\delta) - j C_2 \sin\delta$$
$$E_Y = (C_3 + C_4 \cos\delta) - j C_4 \sin\delta \tag{7}$$

From equations (7) we get

$$\tan \phi_x = \tan (\text{phase of } E_X) = \frac{-C_2}{C_1 + C_2 \cos\delta}$$
$$\tan \phi_y = \tan (\text{phase of } E_Y) = \frac{-C_4}{C_3 + C_4 \cos\delta}$$

From equation (5) we have

$$\tan (\text{phase of } E_X - \text{phase of } E_Y) = \tan \phi \tag{8}$$

or $$\frac{\tan\phi_x - \tan\phi_y}{1 + \tan\phi_x \tan\phi_y} = \tan\phi \qquad (9)$$

Finally substituting (8) into (9) and simplifying we get

$$\tan\phi = \frac{\sin\delta \sin 2(Q-P)}{\cos 2(Q-P)} = \sin\delta \tan 2(Q-P)$$

For a perfect QWP $\delta = 90^\circ$ and our QWP was set with $Q = -45^\circ$ and hence

$$\tan\phi = \tan\left(-\frac{\pi}{2} - 2P\right)$$

Hence $$\phi = -\frac{\pi}{2} - 2P \pm n\pi \qquad n=0,1,2,.....$$

If ϕ_i, P_i are the phase change and polariser reading before optical damage as the laser light traversed the crystal and ϕ_f, P_f are the phase change and polariser reading after optical damage, then

$$\phi_i = -\frac{\pi}{2} - 2P_i \pm n\pi$$

$$\phi_f = -\frac{\pi}{2} - 2P_f \pm n\pi \qquad n=0,1,2,3.....$$

or $$(\phi_f - \phi_i) = 2(P_i - P_f)$$

The phase change ϕ is related to the refractive index of the crystal by

$$\phi = \frac{2\pi}{\lambda} d\,(n_e - n_o)$$

where d = thickness of crystal as traversed by the laser beam

λ = vacuum wavelength of the laser light

n_e = extraordinary refractive index

n_o = ordinary refractive index

$(n_e - n_o)$ is called the birefringence of the crystal.

Hence $$\phi_i = \frac{2\pi}{\lambda} d\,(n_e - n_o)$$

$$\phi_f = \frac{2\pi}{\lambda} d\,[\,(n_e - n_o) + \Delta(n_e - n_o)\,]$$

where $\Delta(n_e-n_o)$ is the change in birefringence due to optical damage. Subtracting we get

$$(\phi_f - \phi_i) = \frac{2\pi}{\lambda} d\, \Delta(n_e-n_o) \qquad (11)$$

Combining equations (10) and (11) we finally get

$$\Delta(n_e-n_o) = \frac{(P_i-P_f)\lambda}{\pi d} \qquad (12)$$

Equation (12) is the basic equation relating the refractive index change due to optical damage and the polariser readings.

5. Balancing Procedure

After the balancing program is loaded into the computer and started, the various pointers are initialised. The computer then waits until an instruction is typed on the keyboard of the teletype. There are several instructions which can be issued; undecoded instructions are ignored. Under normal balancing, the instruction BE is issued (BE = balance ellipsometer) and the polariser is balanced first. The program determines which way it must step the stepping motor of the polariser in order to minimise the error signal of the photomultiplier. It steps the motor in that direction until a set of 64 photomultiplier readings are taken (one after each step) and summed. The motor continues stepping until the error signal goes through a minimum and starts to increase again. A second sum of readings are then taken as the motor steps and is continuously updated to contain only the 64 most recent readings. When this second sum equals the first sum found on the other side of the minimum, the balance point, which is midway between the two equal sums, has been found. The analyser is then balanced in the same

manner. The polariser is then again balanced. The polariser and analyser readings are then printed out on the teletype.

III. CIRCULAR LASER BEAM EXPERIMENT

1. Experiments

Figure 1 shows a map of the change in birefringence $\Delta(n_e-n_o)$ when the crystal is damaged by the argon-ion laser (output=200 mW, radius of beam=0.5 mm) for 10 seconds. A sectional view of the plot through the c-axis of the crystal is shown in figure 2. One notices that $\Delta(n_e-n_o)$ reverses sign near the beam edge while it remains negative inside the beam diameter. A sectional view at right angles to the c-axis is shown in figure 3 and $\Delta(n_e-n_o)$ stays negative all the way. Figure 4 shows a plot of $\Delta(n_e-n_o)$ versus exposure time for a circular damaging beam (radius=0.5 mm). $\Delta(n_e-n_o)$ is linear in time up to an exposure time of 20 seconds. This corresponds to an exposure energy density of $500 J/cm^2$ which agrees well with previously reported results.

2. Qualitative Explanation

In order to explain optical damage, Chen[10] had to postulate the presence of an internal field E_o of unknown origin in the direction of the c-axis of the crystal. Conduction electrons, photoexcited from traps by laser light of the appropriate wavelength, drift under the influence of this field along the c-axis of the crystal for some distance before being retrapped. Assuming that thermal detrapping is negligible, the electrons stay trapped. The space-charge field E_{sc} set up between the positive ionised centres in the illuminated area and the trapped electrons then gives rise to the observed refractive index change via the linear electro-optic effect of the crystal.

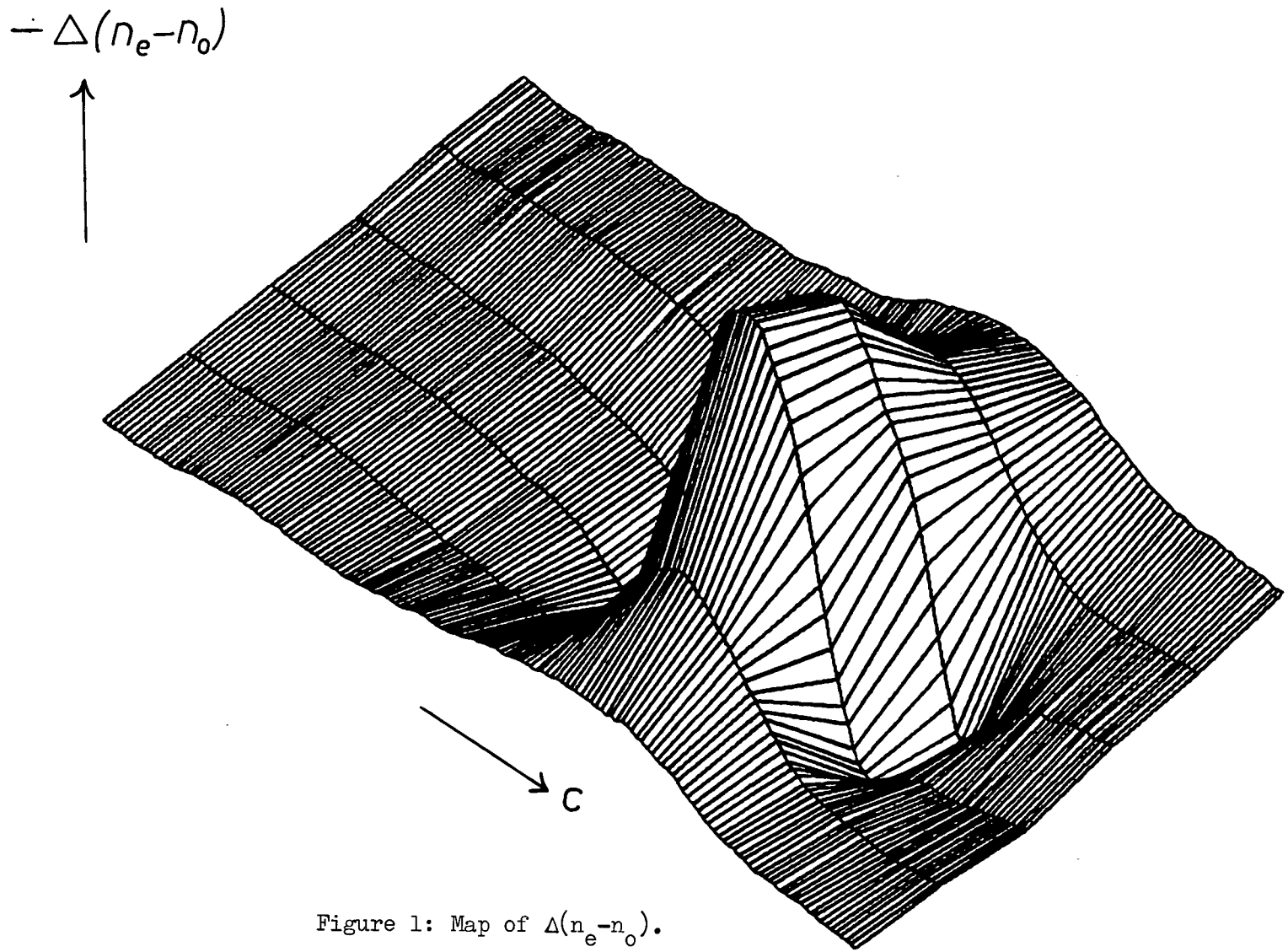

Figure 1: Map of $\Delta(n_e-n_o)$.

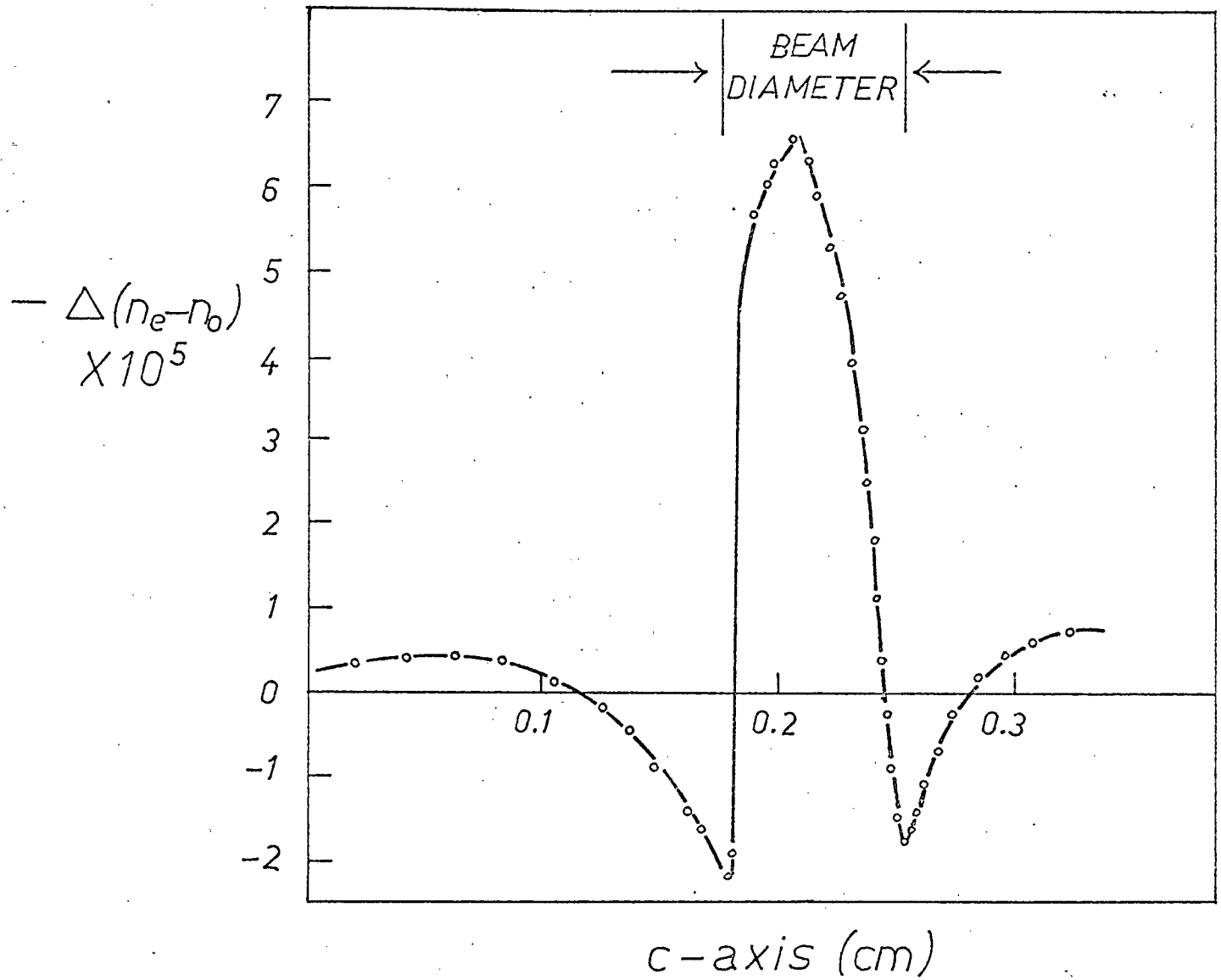

Figure 2: Sectional view through the c-axis of Figure 1.

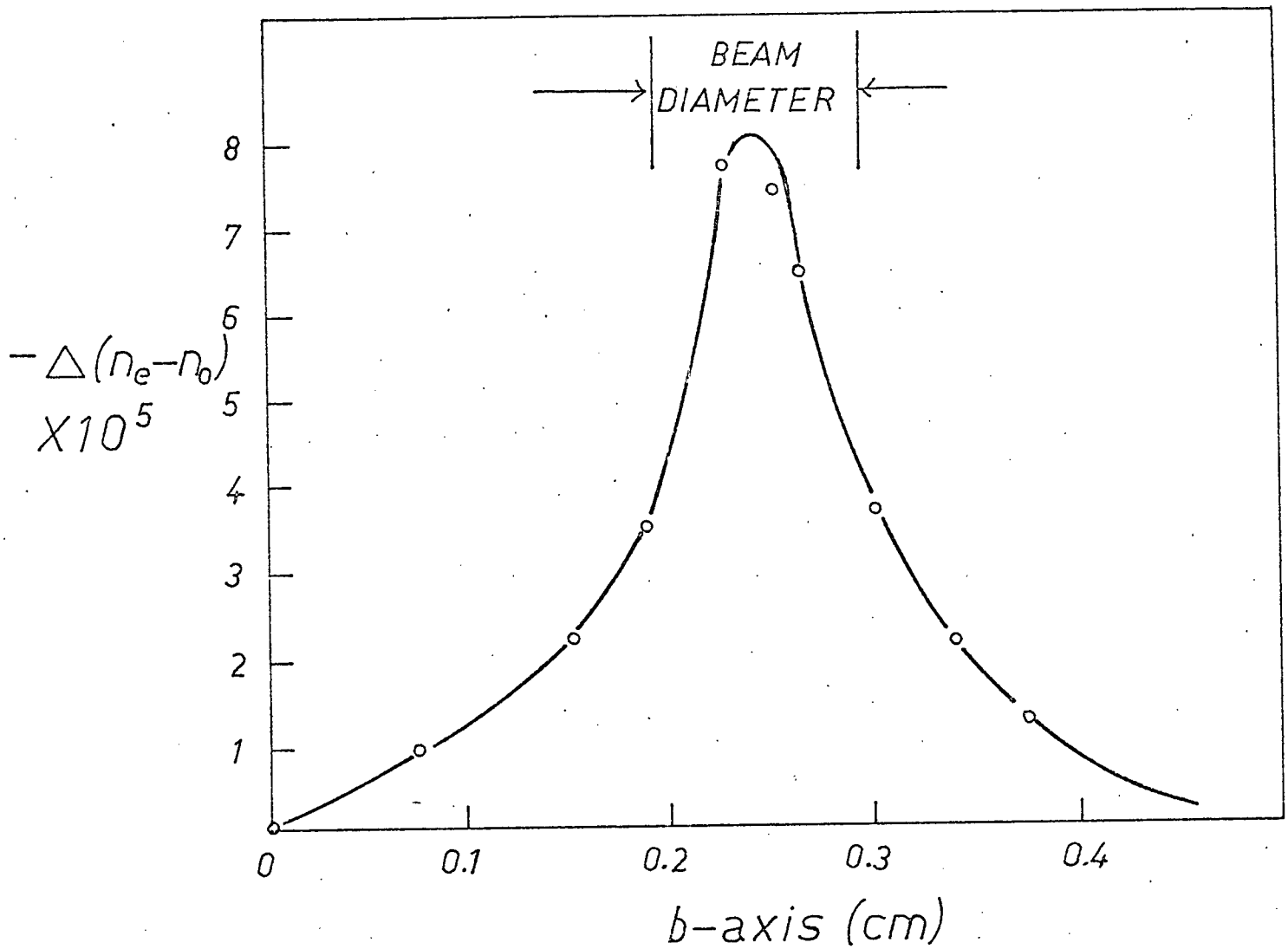

Figure 3: Sectional view through the b-axis of Figure 1.

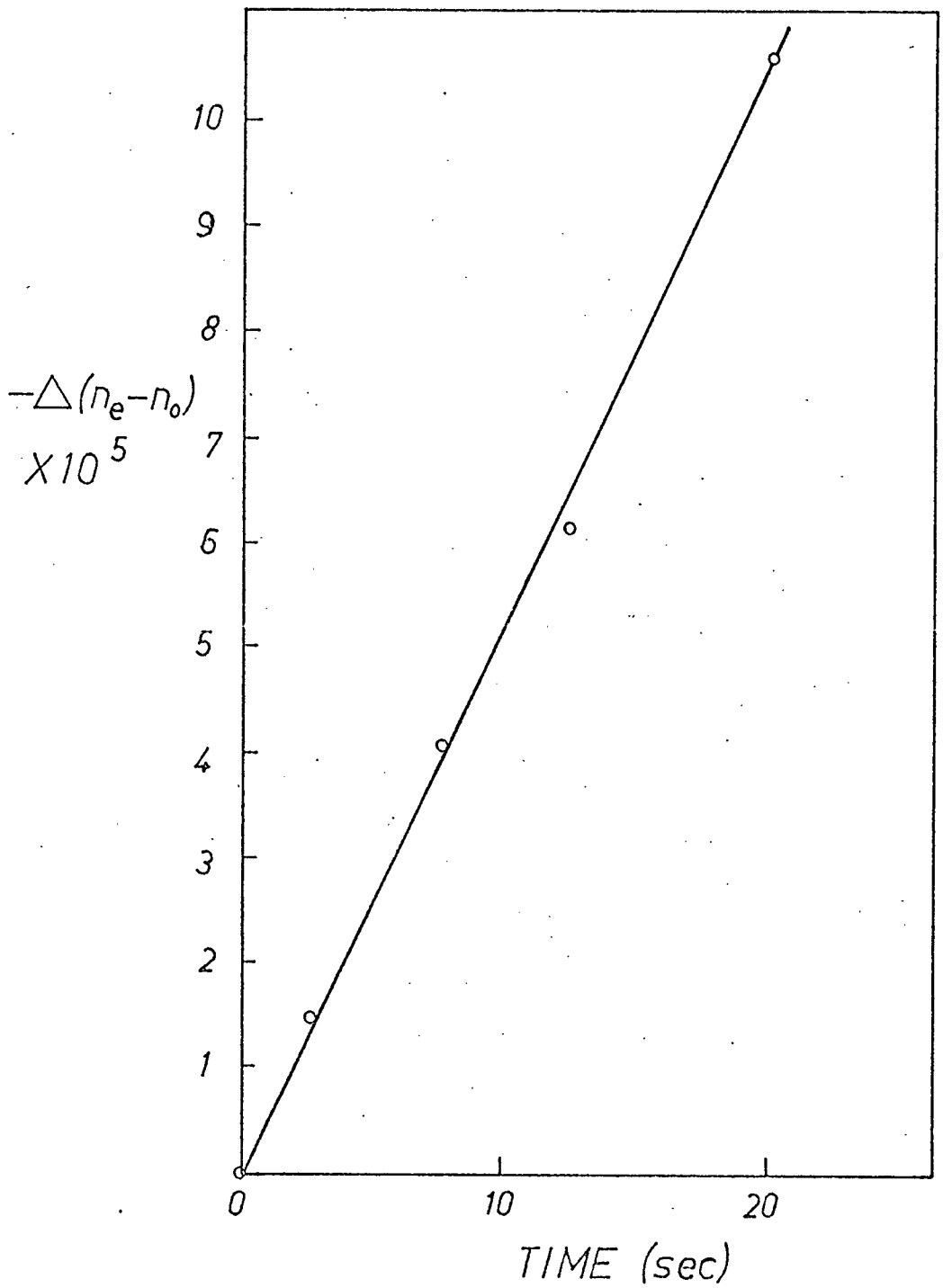

Figure 4: $\Delta(n_e-n_o)$ versus exposure time for a circular beam.

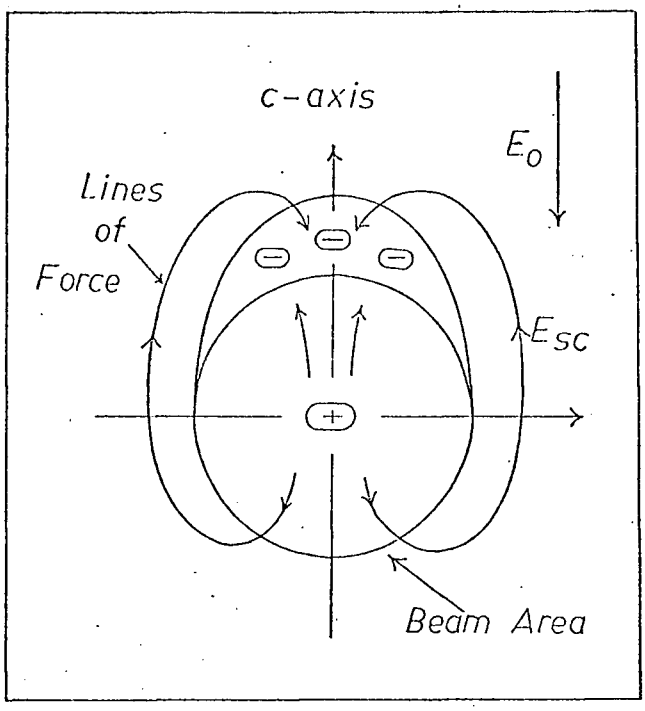

Figure 5: The space-charge field E_{sc} shown in this figure would explain the plot of $\Delta(n_e-n_o)$ of Figures 1,2,3.

Figure 5 indicates situation for a circular damaging beam. It is obvious that the space-charge field (shown here as lines of force) E_{sc} reverses sign along the c-axis but not at right angles to it.

Johnston[11] proposed an alternate theory in which the photo-excitation of electrons by the damaging laser light creates an excess of empty donor sites within the illuminated area and leads to a local increase in the macroscopic polarisation with an accompanying polarisation charge $\rho_p = -\nabla.P \neq 0$. The electric field, due to ρ_p is therefore created antiparallel to the spontaneous polarisation which causes the free carriers to drift along the c-axis until they become retrapped in shallow traps outside the illuminated area. The field, due to the polarisation charge, replaces the internal field E_o postulated by Chen. Steady state is reached when the electric field resulting from the gradient of the polarisation is balanced by the

space-charge field caused by the electrons which have moved out from the illuminated area. The spatially varying polarisation resulting from the change in polarisation described above and the excitation, migration and trapping of electrons induces a spatial variation in the refractive index via the electro-optic effect. According to Amodei[12], the amount of charge transfer involved according to Johnston's theory is too large to be practically realizable.

3. Electro-Optic effect in $LiNbO_3$

The electro-optic effect is defined as the change in the refractive index of a material when a field is applied to it.

For an isotropic medium, the dielectric properties at optical frequencies are given by[13]

$$D = \varepsilon_o \varepsilon E \qquad (1)$$

ε_o = permittivity of free space

ε = dielectric constant of the medium

D = displacement

E = electric field

The refractive index n is defined as

$$n = \sqrt{\varepsilon}$$

For an anisotropic medium equation (1) has to be replaced by

$$D_i = \varepsilon_o \varepsilon_{ij} E$$

It can be shown that for this case two waves, of different velocities, may in general propagate through the crystal for a given wave normal. Each wave has its own refractive index. The principal refractive indices n_1, n_2, n_3 are then accordingly defined as

$$n_1 = \sqrt{\varepsilon_1} \qquad n_2 = \sqrt{\varepsilon_2} \qquad n_3 = \sqrt{\varepsilon_3}$$

where ε_1, ε_2, ε_3 are the principal dielectric constants.

The optical properties of a crystal are often described in terms of the index ellipsoid (indicatrix). The equation of this surface is

$$\frac{x_1^2}{n_1^2} + \frac{x_2^2}{n_2^2} + \frac{x_3^2}{n_3^2} = 1$$

where the co-ordinates x_i are parallel to the axes of the ellipsoid and n_i are the principal refractive indices.

For describing the electro-optic effect where an electric field is applied, the general equation of the indicatrix then becomes

$$\sum_{i,j,k,l} \left[\frac{1}{n_{ij}^2}\delta_{ij} + Z_{ijk}E_k + R_{ijkl}E_kE_l + \ldots\ldots \right] x_ix_j = 1 \qquad (2)$$

where the indices i,j,k,l run from 1 to 3. The Z_{ijk} and R_{ijkl} are linear and quadratic electro-optic tensor components respectively. The indices i,j can be interchanged as can k and l, and the usual contractions can be made

$$r_{mk} \longleftrightarrow Z_{(ij)k} \qquad \text{and} \qquad R_{mn} \longleftrightarrow R_{(ij)(kl)}$$

where m and n run from 1 to 6 and m is related to (ij) and n to (kl) as follows: $1\leftrightarrow 11$, $2\leftrightarrow 22$, $3\leftrightarrow 33$, $4\leftrightarrow 23$, $5\leftrightarrow 13$, $6\leftrightarrow 12$.

For the case of the linear electro-optic effect equation (2) becomes

$$\sum_{i,j,k} \left[\frac{1}{n_{ij}^2}\delta_{ij} + Z_{ijk}E_k \right] x_ix_j = 1$$

The form of the r_{mk} matrix of electro-optic coefficients for $LiNbO_3$ (class 3m) is [13]

$$\begin{bmatrix} 0 & r_{12} & r_{13} \\ 0 & r_{22} & r_{23} \\ 0 & 0 & r_{33} \\ 0 & r_{42} & 0 \\ r_{51} & 0 & 0 \\ r_{61} & 0 & 0 \end{bmatrix}$$

$r_{13} = 8.6 \times 10^{-10}$ cm/Volt

$r_{22} = 3.4 \times 10^{-10}$ cm/Volt

$r_{33} = 30.8 \times 10^{-10}$ cm/Volt

$r_{42} = 2\ 8 \times 10^{-10}$ cm/Volt

Symmetry requires $r_{23} = r_{13}$, $r_{51} = r_{42}$, $r_{22} = -r_{12} = -r_{61}$.

Writing out in full, the equation of the indicatrix for $LiNbO_3$ then becomes

$$\left[\frac{1}{n_1^2} + r_{12}E_2 + r_{13}E_3 \right] x_1^2 + \left[\frac{1}{n_2^2} + r_{22}E_2 + r_{23}E_3 \right] x_2^2$$

$$+ \left[\frac{1}{n_3^2} + r_{33}E_3 \right] x_3^2 + 2r_{61}E_1x_1x_2 + 2r_{42}E_2x_2x_3 + 2r_{51}E_1x_1x_3 = 1$$

where E_1, E_2, E_3 are the electric field strength components in the x_1, x_2, x_3 directions respectively. For a field (either applied or internal) parallel to x_3 (the c-axis of the crystal) the indicatrix becomes

$$\left[\frac{1}{n_1^2} + r_{13}E_3 \right] x_1^2 + \left[\frac{1}{n_2^2} + r_{23}E_3 \right] x_2^2 + \left[\frac{1}{n_3^2} + r_{33}E_3 \right] x_3^2 = 1$$

Thus there are modifications only to the axis length but no rotation of the principal axes of the index ellipsoid.

The indicatrix has the following important properties. If a wavefront has its normal in a certain direction $\vec{P}$, then the two wavefronts normal to $\vec{P}$ which may be propagated through the crystal have

refractive indices equal to the semi-axes of the ellipse obtained in the following way. Draw through the origin of the indicatrix a straight line in the direction of $\vec{P}$. Draw the central section of the indicatrix perpendicular to it. This will be the ellipse whose major and minor axes are the respective indices.

For the experimental set up, a light wave (the probing helium-neon laser) is propagating in the x_2 direction and with space-charge field E_3 in the x_3 direction, the equation for the $x_2 = 0$ section of the indicatrix is

$$\left[\frac{1}{n_1^2} + r_{13}E_3 \right] x_1^2 + \left[\frac{1}{n_3^2} + r_{33}E_3 \right] x_3^2 = 1$$

$LiNbO_3$ is an uniaxial crystal with x_3 as the polar axis and $n_1 = n_o = n_2$, $n_3 = n_e$

Hence $$\left[\frac{1}{n_o^2} + r_{13}E_3 \right] x_1^2 + \left[\frac{1}{n_e^2} + r_{33}E_3 \right] x_3^2 = 1$$

The effect of the field E_3 is thus to change the index of refraction for a wave polarised along x_1 so that the new index $(n_o + \Delta n_o)$ is given by

$$\frac{1}{(n_o + \Delta n_o)^2} x_1^2 = \left(\frac{1}{n_o^2} + r_{13}E_3 \right) x_1^2$$

Since $\Delta n_o << n_o$ we can make the approximation

$$\frac{1}{(n_o + \Delta n_o)^2} = \frac{1}{n_o^2} \left[1 + \frac{\Delta n_o}{n_o} \right]^{-2} \approx \frac{1}{n_o^2} \left[1 - \frac{2\Delta n_o}{n_o} \right]$$

Therefore $$- \frac{2\Delta n_o}{n_o^3} = r_{13}E_3$$

or $$\Delta n_o = - \frac{n_o^3 r_{13} E_3}{2}$$

Similarly for the wave polarised along x_3

$$\Delta n_e = - \frac{n_e^3 r_{33} E_3}{2}$$

Hence $$\Delta(n_e - n_o) = \frac{E_3}{2} (n_o^3 r_{13} - n_e^3 r_{33})$$

At the wavelength of the helium-neon laser (6328 Å)

$n_o = 2.2918$ $\qquad$ $n_e = 2.2012$

$r_{13} = 8.6 \times 10^{-10}$ cm/V $\qquad$ $r_{33} = 30.8 \times 10^{-10}$ cm/V

Substituting we get

$$\Delta(n_e - n_o) = -1.13 \times 10^{-8} E_3$$

4. Quantitative Modelling of Optical Damage

King[8] carried out a quantitative analysis of the light induced refractive index change in KTN where a static external field has to be applied in order for optical damage to occur. He based his analysis on Chen's theory. Neglecting diffusion effects, electrons which are photo-excited drift and become retrapped and their concentrations are assumed to remain small compared to the donor and trap densities. Furthermore, King assumed that the drift length of electrons is small compared to the scale of refractive index change so that the electron concentration always remains proportional to the light intensity and is given by:

$$n_o(x,y) = \left[\frac{2P_o \alpha \tau}{\pi h\nu r_o^2}\right] \exp\left[\frac{-2(x^2+y^2)}{r_o^2}\right]$$

where P_o = power of laser beam

$h\nu$ = photon energy

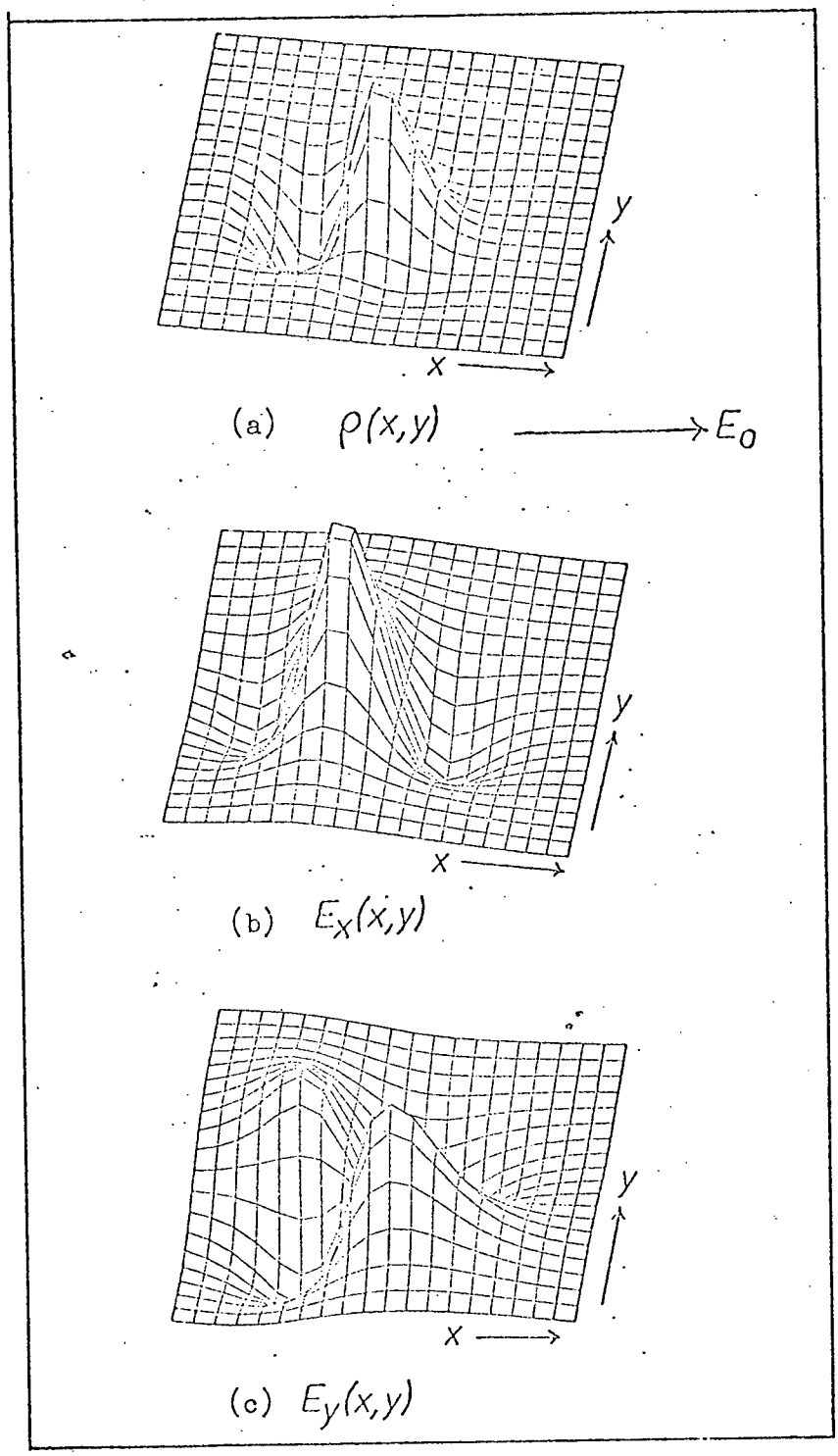

Figure 6: Three-dimensional plots showing the spatial distribution of (a) the space charge with hills and valleys signifying positive and negative charge, (b) the x component of the internal field and (c) the y component of the internal field.

τ = electron life time

r_o = laser beam radius

α = optical absorption at the damaged wavelength

The equation of continuity requires

$$\frac{\partial \rho}{\partial t} = - \nabla . \vec{J} \qquad (2)$$

and $$\vec{J} = q n_o u (\vec{E}_o + \vec{E}_{sc}) \qquad (3)$$

where ρ = charge density

q = electron charge

u = mobility of electron

$\vec{E}_o$ = internal field

$\vec{E}_{sc}$ = space-charge field

Equations (1), (2) and (3) together with Poisson's equation

$$\nabla . \vec{E} = \nabla . (\vec{E}_o + \vec{E}_{sc}) = \nabla . \vec{E}_{sc} = \frac{\rho}{\varepsilon_o \varepsilon_r}$$

enables us to solve for $\vec{E}_{sc}$.

Now, the formal solution to (4) is

$$\vec{E}_{sc}(x,y,t) = \frac{1}{2\pi\varepsilon_o\varepsilon_r} \nabla_{x,y} \iint \rho(x',y',t) \ln|\vec{r}| \, dx'dy'$$

where r is the distance from (x', y') to (x, y).

The above equations have been solved using finite difference methods . Appendix A outlines the method used and also contains a copy of the program written to solve the above equations. Figure 6 show a three-dimensional plot of $\rho(x,y)$, $E_x(x,y)$, $E_y(x,y)$ after 12 iterations using the following constants

$\alpha u \tau$ = 10^{-10} m/V

P_o = 10^{-3} Watts

ν = 2.08 x 10^{15} cycles/sec

$h = 1.2 \times 10^{-5}$ m

$r_o = 10^{-4}$ m

$E_o = 4 \times 10^5$ v/m

$\Delta t = 1.0$ sec

$\varepsilon_o \varepsilon_r = 2.83 \times 10^{-10}$ F/m

where $E_x(x,y)$ and $E_y(x,y)$ are the x and y components of the space-charge field E_{sc}.

One notices that $E_x(x,y)$ indeed shows the same feature as Figure 1. Along the x direction, $E_x(x,y)$ reverses sign at the beam edge whereas along the y direction $E_x(x,y)$ stays unchanged in sign.

King was able to obtain numerical values of $\alpha\mu\tau$ since E_o is a known constant in his case. For the case of $LiNbO_3$, both $\alpha\mu\tau$ and E_o are unknowns and hence unless $\alpha\mu\tau$ and E_o can be determined independently, it is not possible to solve for these two quantities from the numerical analysis.

IV. NARROW SLIT EXPERIMENT

1.1 Slit perpendicular to the c-axis

The holographic storage mechanism in lithium niobate can further be investigated by using different geometry for the damaging laser beam. Referring to Figure 1, if a narrow strip of laser light is placed across the crystal in a direction perpendicular to that of the proposed internal field E_o, then, for a sufficiently narrow slit, we expect a one-dimensional problem along the c-axis where drift due to E_o would be the dominant mechanism affecting the movement of photo-excited electrons. This is a simpler problem to analyse than the previous case where the fact that it is a two-dimensional problem makes it more difficult to solve. Further, in the analysis by King, he has to assume that the diffusion and drift lengths are both small so that $n_o(x,y)$ always remains proportional to the light intensity. No such assumption is required in the one-dimensional case.

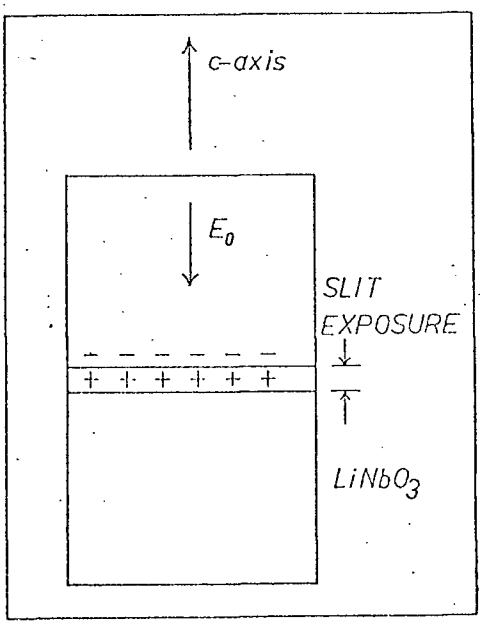

Figure 1: For a sufficiently narrow strip of light placed across the crystal as shown, drift would be the dominant mechanism affecting the movement of electrons along the c-axis.

1.2 Theory

A considerable simplication is obtained when the problem is made spatially one-dimensional. Further simplification is obtained if the exposure (time x intensity) is kept small enough for the effects causing saturation to be neglected. This means:

(1) the space-charge field E_{sc} set up between the positive ionised centres in the illuminated area and the trapped electrons is neglected compared to the internal field E_o,

(2) the trap occupancy is considered to be only slightly perturbed, so that

  (a) the rate of release of electrons from traps at a given point remains proportional to the light intensity at that point, and

  (b) the rate of capture of conduction band electrons by traps is proportional to their concentration.

Using these assumptions, the treatment is applicable to the initial linear part of the hologram-writing process illustrated in Figure 4 of Chapter III. We have two simple cases.

(1) With a narrow strip of laser light perpendicular to the c-axis. In this case, the motion of electrons along the c-axis is due chiefly to drift resulting from E_o.

(2) With a narrow strip of laser light parallel to the c-axis. In this case, diffusion is the dominant mechanism affecting the movement of electrons in a direction perpendicular to the c-axis

Under the above assumptions, the following equations governing optical damage can be written down:

$$\vec{J} = ne\mu_n (\vec{E}_o + \vec{E}_{sc}) + eD_n \nabla n \sim ne\mu_n \vec{E}_o \quad (1)$$

$$\frac{\partial n}{\partial t} = -\frac{n}{\tau} + \frac{1}{e} \nabla . \vec{J} + g(\text{light}) \quad (2)$$

$$\frac{\partial \rho}{\partial t} = -\nabla . \vec{J} \quad (3)$$

$$\nabla . \vec{E}_{sc} = \rho / \varepsilon_o \varepsilon \quad (4)$$

Equation (1) is the current density equation where the diffusion term is neglected.

Equations (2) and (3) are the continuity equations for the concentration of electrons and the current density respectively.

Equation (4) is Poisson's equation.

For the one-dimensional problem, these equations simplify to

$$J(x,t) = ne\mu_n E_o \quad (5)$$

$$\frac{\partial n(x,t)}{\partial t} = -\frac{n(x,t)}{\tau} + \frac{1}{e}\frac{\partial J}{\partial x} + g(\text{light}) \quad (6)$$

$$\frac{\partial \rho(x,t)}{\partial t} = -\frac{\partial J(x,t)}{\partial x} \quad (7)$$

$$\frac{\partial E_{sc}}{\partial x} = \frac{\rho(x,t)}{\varepsilon_o \varepsilon} \quad (8)$$

where $J(x,t)$ = electron current density

E_o = internal field

$n(x,t)$ = concentration of electrons in the conduction band

e = electron charge

$\rho(x,t)$ = charge density

ε_o = permittivity of free space

ε = dielectric constant of medium

$g(\text{light})$ = rate of generation of electrons due to laser light

For the problem of holography g(light) may be a complicated expression of the spatial variable which may be known only graphically. As indicated below, the Laplace transform method is particularly suitable for solving the problem of arbitrary g(light). Thus, although the original problem can easily be solved using elementary methods, the Laplace transform method is used.

The bilateral Laplace transform $\mathcal{L}$ of a function f(x) is defined as:

$$\mathcal{L}[\, f(x)\,] = \int_{-\infty}^{\infty} f(x)\, e^{-sx}\, dx = F(s)$$

In the steady state $\dfrac{\partial n(x,t)}{\partial t} = 0$

Substituting equation (5) into (6) and taking Laplace transform (with respect to the spatial variable x) of the resulting equation we get

$$0 = -\frac{N(s)}{\tau} + s\,\mu_n E_o\, N(s) + G(s)$$

where

$$N(s) = \mathcal{L}[n(x,t)]$$

$$G(s) = \mathcal{L}[g(\text{light})]$$

Hence

$$N(s) = \frac{1}{E_o\left[-s + \dfrac{1}{\mu_n E_o \tau}\right]}\, G(s) = H(s)\, G(s)$$

and $n(x,t) = h(x) * g(\text{light})$

where

$$h(x) * g(\text{light}) = \int_{-\infty}^{\infty} g(y)\, h(x-y)\, dy = \text{convolution of } g(\text{light}) \text{ and } h(x)$$

and h(x) is the inverse Laplace transform of H(s) and is given by

$$h(x) = \frac{u(-x)}{\mu_n E_o} \exp \frac{x}{\mu_n E_o \tau}$$

where u(x) is a unit step function. h(x) is shown in Figure 2.

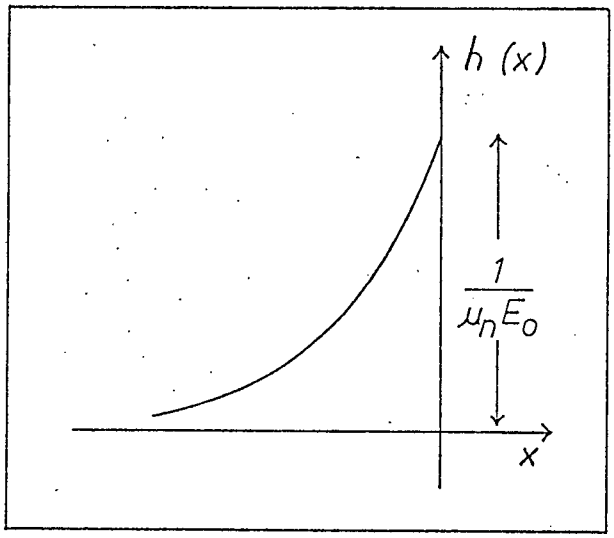

Figure 2: Plot of h(x).

Thus we see that for arbitrary g(light), n(x,t) is obtained by the convolution of h(x) and g(light), either graphically or analytically.

For the irradiating geometry of Figure 1, g(light) is given by

$$g(\text{light}) = A \qquad -d/2 < x < d/2$$

where A is a constant, the convolution can be carried out analytically. $E_{sc}(x)$ is then obtained from n(x,t) by combining equations (5),(7) and (8) to yield

$$E_{sc}(x) = - \frac{n(x,t)\ e\ E_o\ t\ \mu_n}{\varepsilon_o \varepsilon}$$

Carrying out the computations we finally get:

$$n(x,t) = 2A\tau \exp\frac{x}{\mu_n E_o \tau} \sinh\frac{d}{2\mu_n E_o \tau} \qquad x < -d/2$$

$$= A\tau\left[1 - \exp\frac{-d}{2\mu_n E_o \tau} \exp\frac{x}{\mu_n E_o \tau}\right] \qquad -d/2 < x < d/2$$

$$= 0 \qquad x > d/2$$

$$E_{sc}(x) = -\frac{2e\mu_n}{\varepsilon_o \varepsilon} E_o tA\tau \exp\frac{x}{\mu_n E_o \tau} \sinh\frac{d}{2\mu_n E_o \tau} \qquad x < -d/2$$

$$= -\frac{1}{\varepsilon_o \varepsilon} A e \mu_n E_o t\left[1 - \exp\frac{-d}{2\mu_n E_o \tau} \exp\frac{x}{\mu_n E_o \tau}\right] \qquad -d/2 < x < d/2$$

$$= 0 \qquad x > d/2$$

$g(x)$, $n(x)$ and $E_{sc}(x)$ are plotted in Figure 3 for the case of a slit perpendicular to the c-axis.

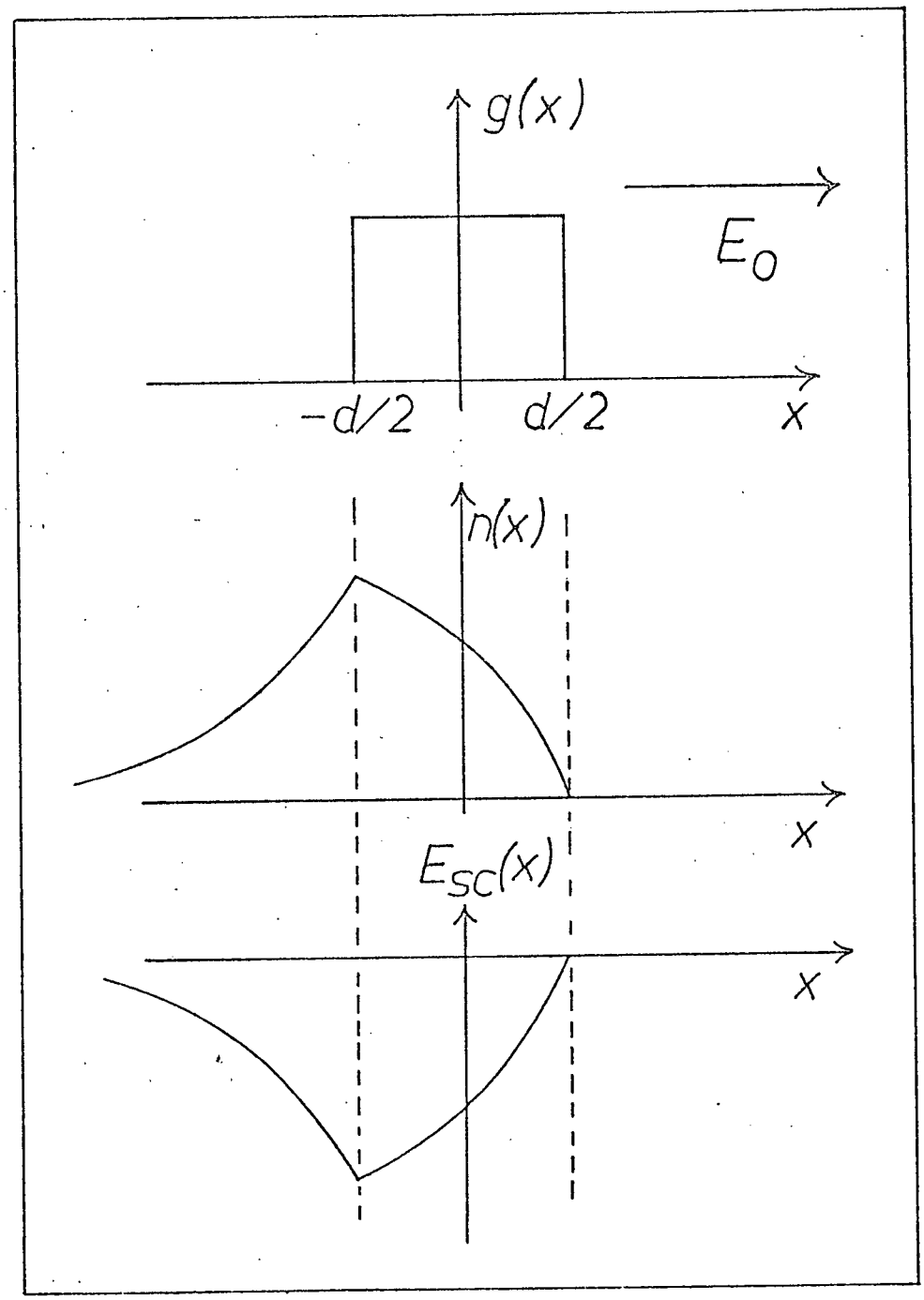

Figure 3: Plot of g(x), n(x) and $E_{sc}(x)$, the steady state solution of the problem formulated in section 1.2 .

1.3 Experimental Results

Figure 4 shows a plot of $-\Delta(n_e-n_o)$ versus distance along the c-axis for a slit width of 0.06 $\pm$ 0.002cm (Power = 200mW). Comparing this plot with the plot of $E_{sc}(x)$ of Figure 3., one notices two anomalies: $\Delta(n_e-n_o)$ remains slightly positive on one end of the slit and the maximum of $\Delta(n_e-n_o)$ does not exactly occur at the slit edge as predicted by theory. The anomalies are probably due to experimental errors. From Figure 4 and the theory, a value of $\mu_n \tau E_o = 0.09 \pm 0.005$ cm is obtained.

2.1 Slit parallel to c-axis

On the other hand, if the slit of light is placed across the crystal in the direction of the c-axis (Figure 5); then, again for a sufficiently narrow slit, we expect a one-dimensional problem in a direction perpendicular to the c-axis and since there is no field in this direction, diffusion is now the dominant mechanism governing the movement of electrons. However, electrons are not expected to move very far by diffusion and hence it was not surprising that experimentally we have so far observed no effect with this geometry. The diffusion length is probably too small to be resolved under our present experimental instrumentation. However, the one-dimensional probelm has been solved analytically in the next section.

2.2 Theory

The assumptions made to solve this problem are the same as the previous case except that diffusion, and not drift, dominates the movement of electrons. Except for equation (1), the remaining three equations remain unchanged.

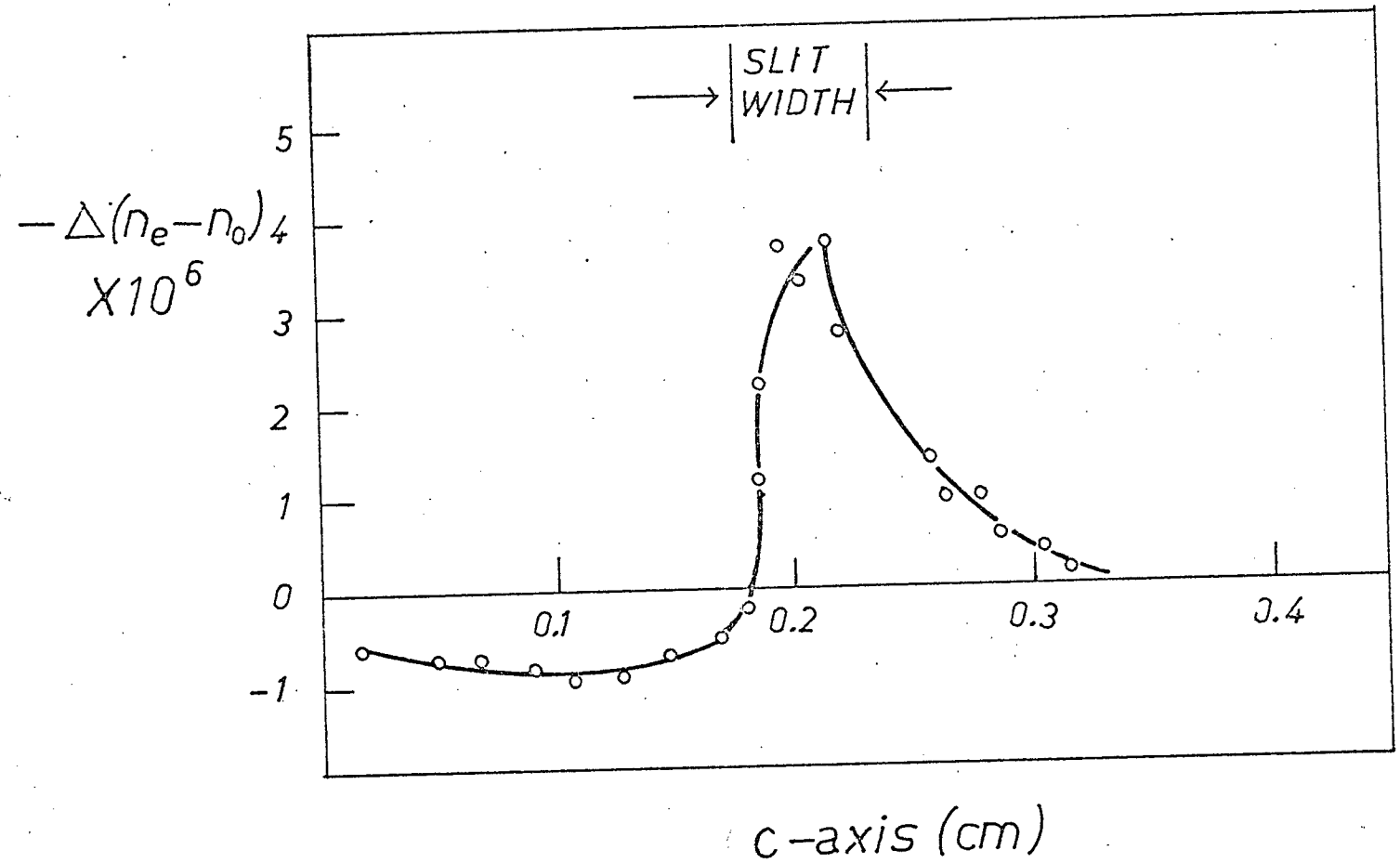

Figure 4: Plot of $\Delta(n_e-n_o)$ along the c-axis for a slit width of 0.06 $\pm$ 0.002 cm.

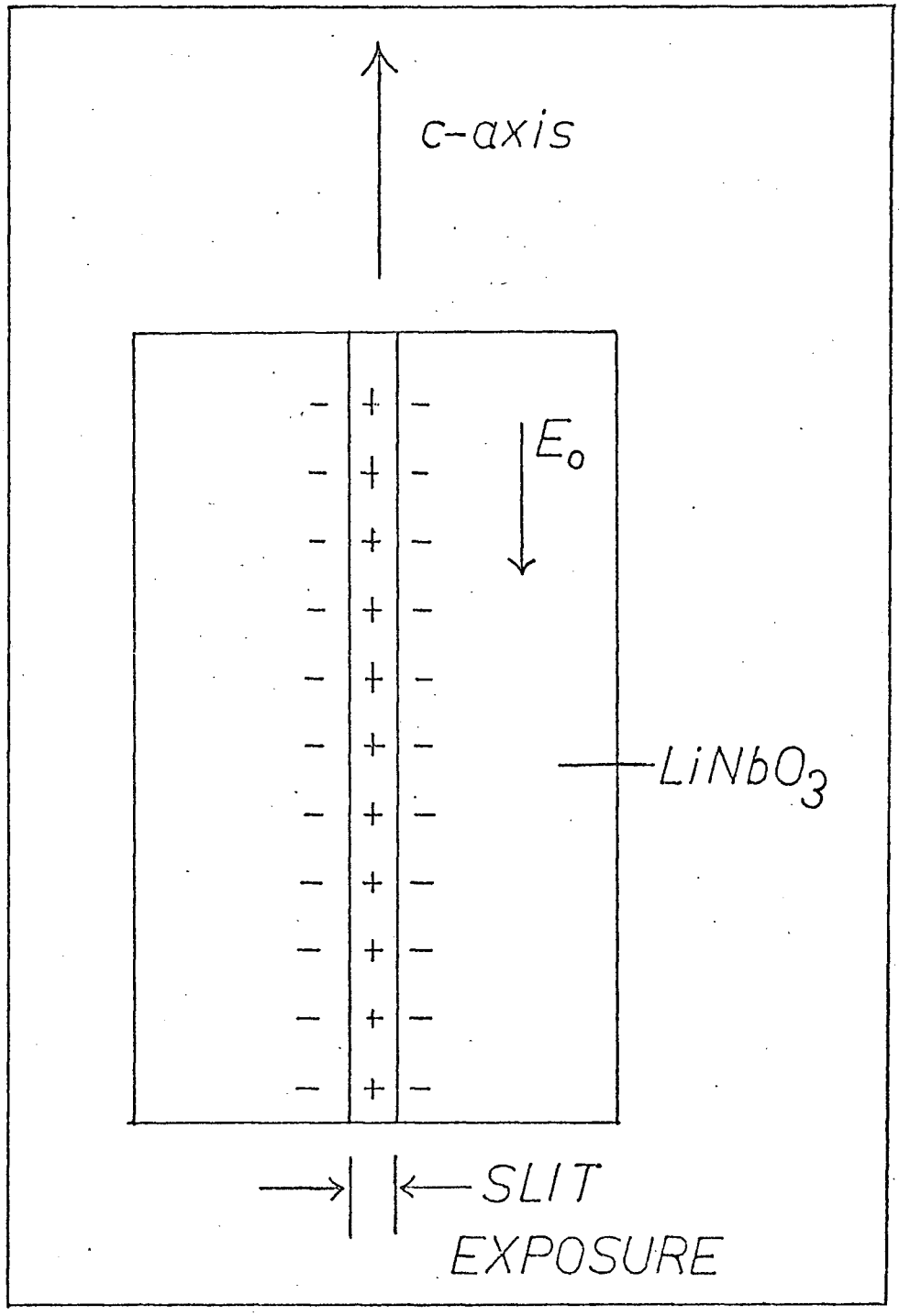

Figure 5: For a sufficiently narrow strip of light placed across the crystal as shown, diffusion would be the dominant mechanism affecting the movement of electrons in a direction perpendicular to the c-axis.

$$J = eD_n \frac{\partial n}{\partial x} \tag{1}$$

$$\frac{\partial n}{\partial t} = -\frac{n}{\tau} + \frac{1}{e}\frac{\partial J_n}{\partial x} + g(\text{light}) \tag{2}$$

$$\frac{\partial \rho}{\partial t} = -\frac{\partial J}{\partial x} \tag{3}$$

$$\frac{\partial E_{sc}}{\partial x} = \frac{\rho}{\varepsilon_o \varepsilon} \tag{4}$$

Again, the steady state solution is solved using Laplace transform method. Substituting equation (1) into (2) and taking Laplace transform (with respect to the spatial variable x) of the resulting equation we get

$$0 = -\frac{N(s)}{\tau} + D_n s^2 N(s) + G(s)$$

where $N(s) = \mathcal{L}[n(x)]$

$G(s) = \mathcal{L}[g(\text{light})]$

Hence $$N(s) = \frac{-\tau}{(D_n \tau s^2 - 1)} G(s) = H(s)\, G(s)$$

and $$n(x) = h(x) * g(\text{light})$$

where $h(x)$ is the inverse Laplace transform of $H(s)$ and is given by

$$h(x) = \frac{1}{2}\sqrt{\frac{\tau}{D_n}} \left[\exp \frac{-x}{\sqrt{D_n \tau}}\, u(x) + \exp \frac{x}{\sqrt{D_n \tau}}\, u(-x) \right]$$

$$= h_1(x) + h_2(x)$$

$h(x)$, $h_1(x)$ and $h_2(x)$ are plotted as shown in Figure 6.

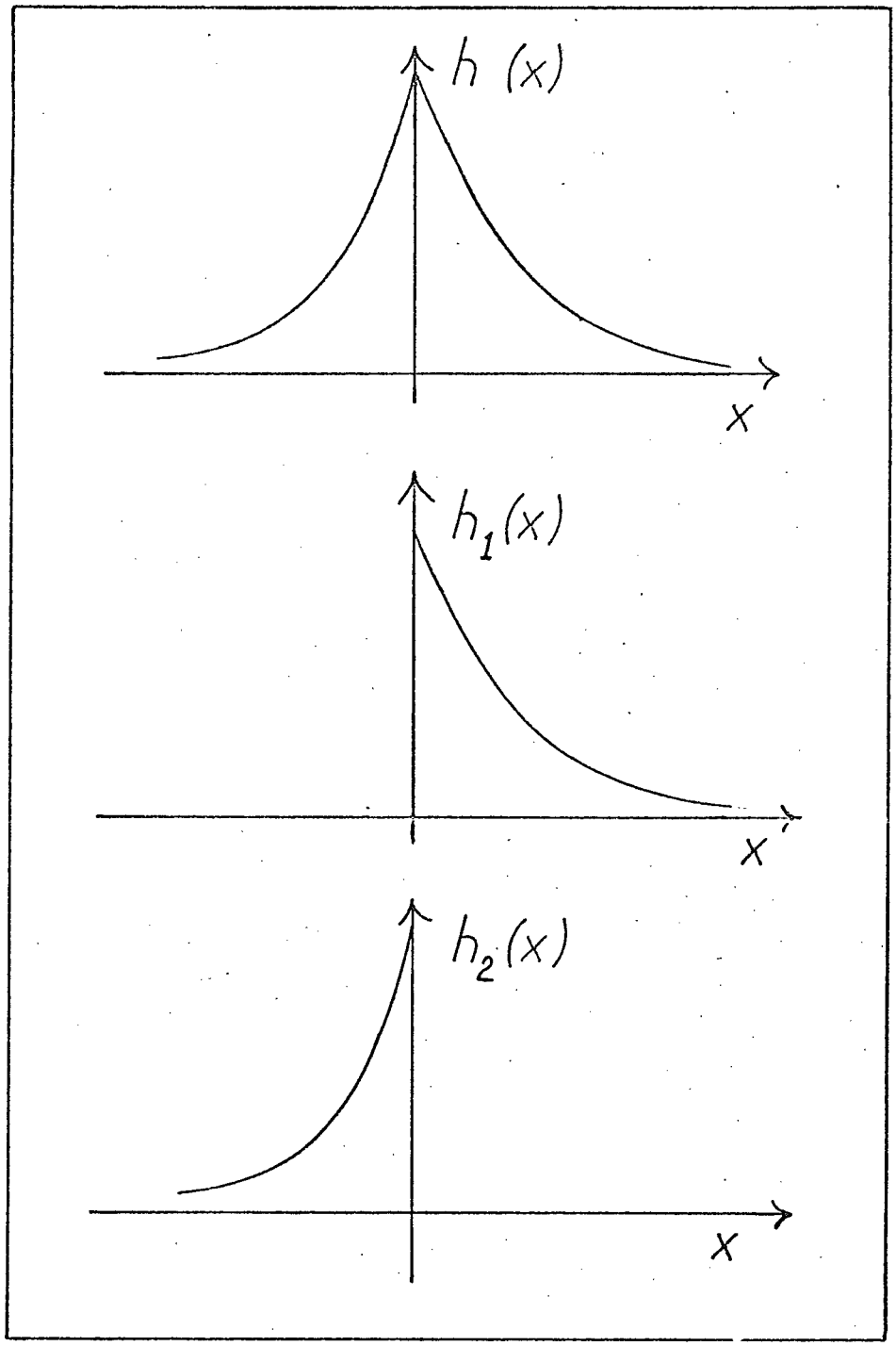

Figure 6: Plot of h(x), $h_1(x)$ and $h_2(x)$

Thus we see that for arbitrary g(light), n(x) is obtained by the convolution of h(x) and g(light), either graphically or analytically. Notice that h(x) is made up of two simple exponentials, $h_1(x)$ and $h_2(x)$, so that the convolution is essentially the same as the previous case.

For the irradiating geometry of Figure 5, g(light) is given by

$$g(\text{light}) = A \qquad -d/2 < x < d/2$$

Performing the convolution integrals separately for $h_1(x)$ and $h_2(x)$ we get

$$n(x) = A\tau \exp \frac{x}{\sqrt{D_n \tau}} \sinh \left(\frac{d}{2\sqrt{D_n \tau}} \right) \qquad x < -d/2$$

$$= A\tau \left[1 - \exp \frac{-d}{2\sqrt{D_n \tau}} \cosh \frac{x}{\sqrt{D_n \tau}} \right] \qquad -d/2 < x < d/2$$

$$= A\tau \exp \frac{-x}{\sqrt{D_n \tau}} \sinh \frac{d}{2\sqrt{D_n \tau}} \qquad x > d/2$$

Having solved for n(x), $E_{sc}(x)$ can again be solved. Combining equations (1), (3) and (4) we have

$$E_{sc}(x) = - \frac{eD_n t}{\varepsilon_o \varepsilon} \frac{\partial n(x)}{\partial x}$$

Substituting for n(x) from above we have

$$E_{sc}(x) = \frac{-eAt}{\varepsilon_o \varepsilon} \sqrt{D_n \tau} \exp \frac{x}{\sqrt{D_n \tau}} \sinh \left(\frac{d}{2\sqrt{D_n \tau}} \right) \qquad x < -d/2$$

$$= \frac{eAt}{\varepsilon_o \varepsilon} \sqrt{D_n \tau} \exp \frac{-d}{2\sqrt{D_n \tau}} \sinh \left(\frac{x}{\sqrt{D_n \tau}} \right) \qquad -d/2 < x < d/2$$

$$= \frac{eAt}{\varepsilon_o \varepsilon} \sqrt{D_n \tau} \exp \frac{-x}{\sqrt{D_n \tau}} \sinh \left(\frac{d}{2\sqrt{D_n \tau}} \right) \qquad x > d/2$$

g(x), n(x) and $E_{sc}(x)$ are plotted in Figure 7.

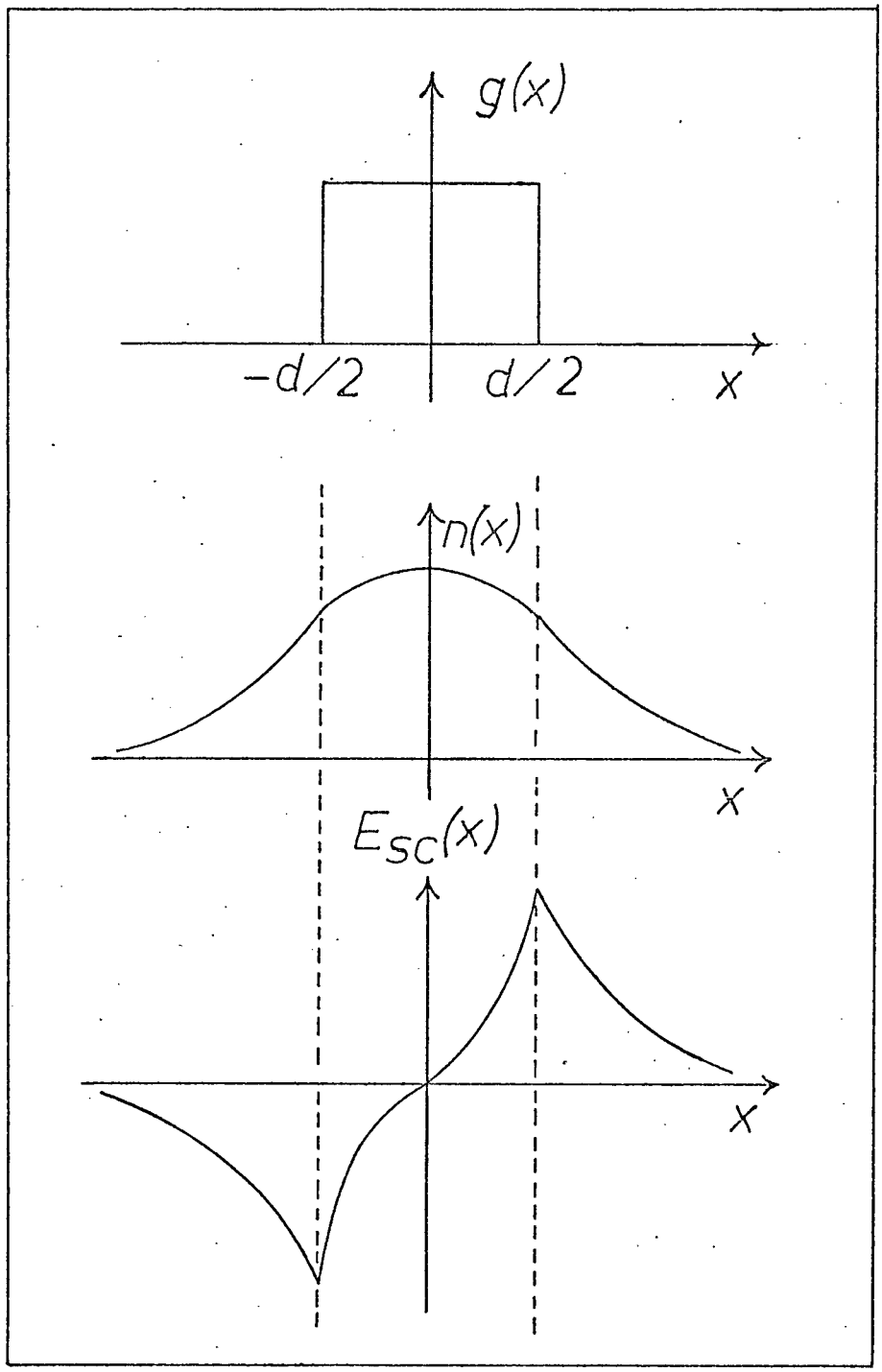

Figure 7: Plot of g(x), n(x) and $E_{sc}(x)$, the steady state solution of the problem formulated in section 2.2 .

3. Further Experiment to investigate internal field

The built-in field postulated by Chen may further be investigated as follows. If one scans along the c-axis of the crystal so as to get a map of the birefringence (n_e-n_o), then any variations in (n_e-n_o) along the c-axis may give an indication of the variations in E_o. The variations in (n_e-n_o) may also be the result of non-stoichiometry caused by changes in the composition of the crystal during the growth process.[14] A plot of (n_e-n_o) along the c-axis is shown in figure 8 (solid line). The point of zero field is undetermined. By putting electrodes across opposite end of the crystal and shorting the electrodes, we expect to make the average field $\int Edx$ along the c-axis zero. If the variations in (n_e-n_o) are not due to non-stoichiometry, then from the curve shown one would expect that the point of zero field would be roughly in the middle of the crystal (since (n_e-n_o) increases quite smoothly along the c-axis). (n_e-n_o) after shorting the electrodes is also shown in figure 8 as a dotted line. It can be seen that (n_e-n_o) remains almost unchanged. (The maximum shift in (n_e-n_o) is 8.2×10^{-6} which corresponds to a shift in the internal field of 800V/cm.) This indicates that the average field $\int Edx$ along the c-axis is almost zero even before shorting the electrodes. By repeating the circular damaging beam experiments but with the beam placed in 3 places along the c-axis where E_o is negative, zero and positive, one would expect then that $\Delta(n_e-n_o)$ would also reverse sign at the two spots where E_o reverse sign and remains zero where E_o is zero. The experimental results are shown in figure 9 where it is obvious that $\Delta(n_e-n_o)$ did not reverse sign. This could be explained if the internal field varies along the c-axis as shown in figure 10 where to meet the requirements of $\int Edx = 0$ with the electrodes shorted, the shaded area must be equal

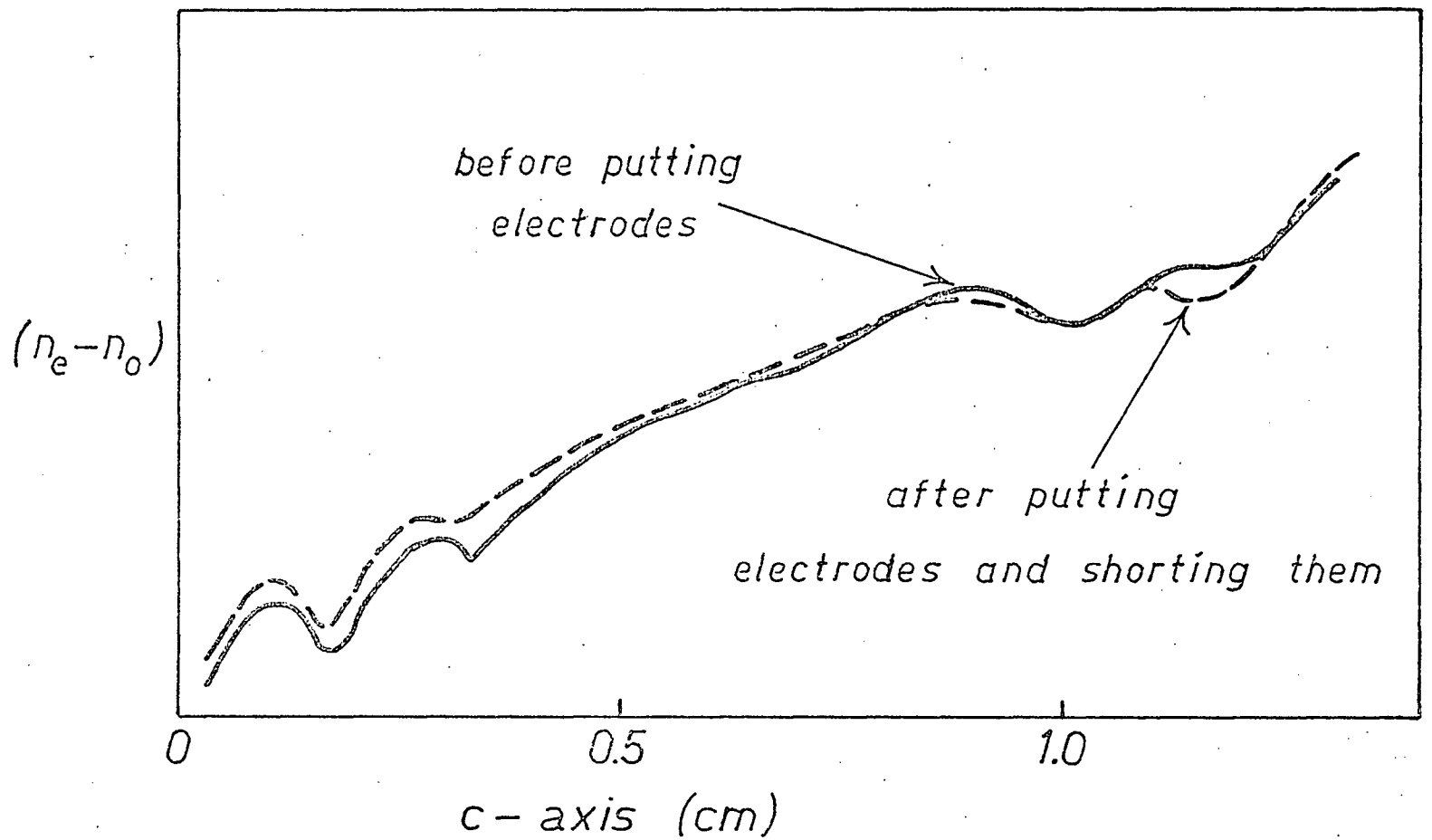

Figure 8: Plot of (n_e-n_o) along the c-axis before depositing electrodes (solid line) and after depositing electrodes and shorting them (dotted line).

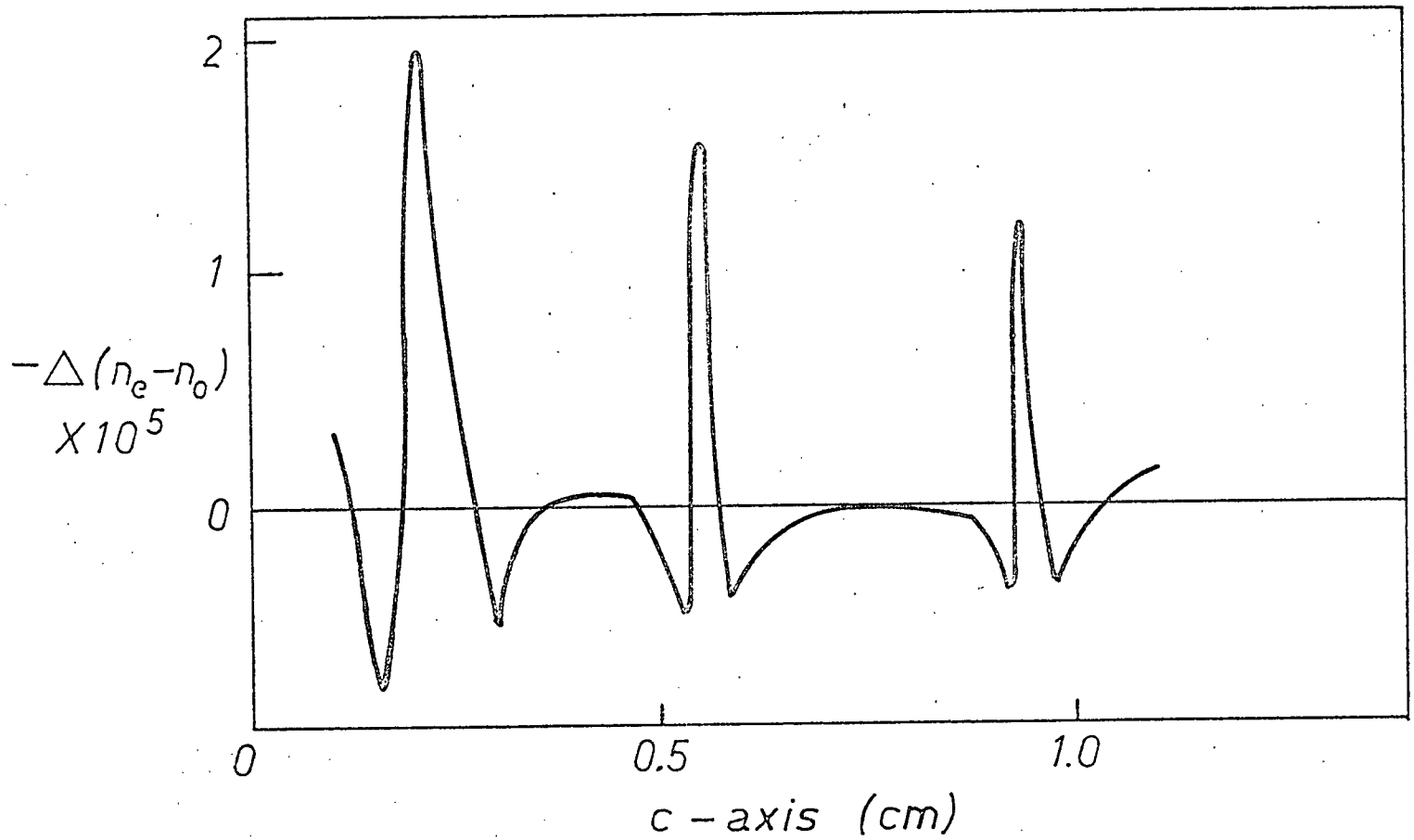

Figure 9: Plot of $\Delta(n_e-n_o)$ for a circular damaging beam placed at 3 places along the c-axis.

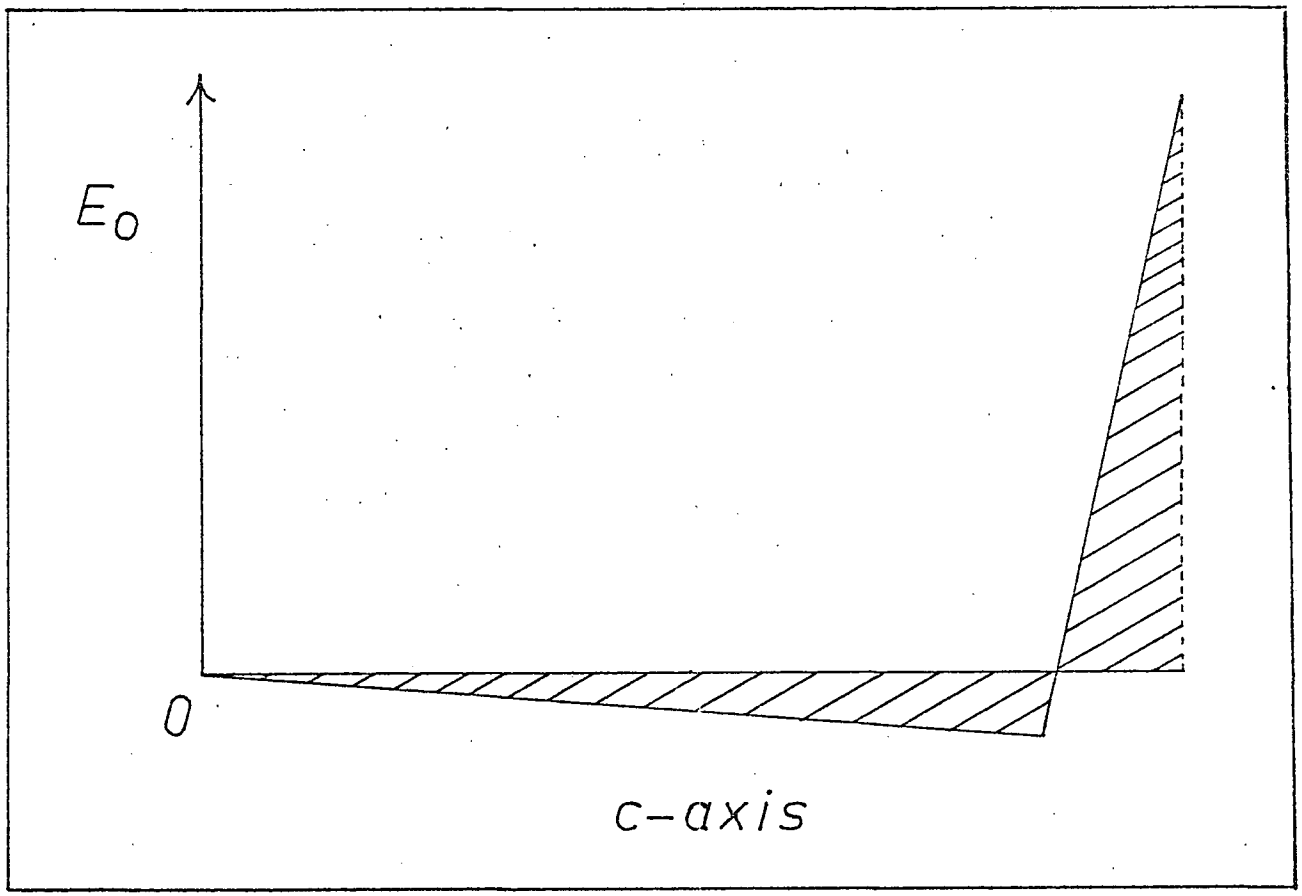

Figure 10: Variations of E_o along the c-axis to satisfy the criterion that $\int Edx = 0$ along the c-axis.

V. CONCLUSIONS

The optical damage process in lithium niobate has been investigated. The automated ellipsometer is used for studying the process because the birefringence of the crystal can readily be determined and the balancing procedure would be extremely tedious if done by hand. Further, the angles of the polariser and analyser can be read to a sensitivity of $\pm$ 0.01^{o} which corresponds to 10^{-7} in (n_e-n_o) for the specimen thickness used.

It was found that consistency of experimental results was obtained by baking the crystal and cooling it slowly before each experiment so as to anneal out the space-charge field created during optical damage of previous experiments. The cooling of the crystal after baking had to be carried out slowly, otherwise random pyroelectric field might be frozen in the crystal.

To verify Chen's model of the existence of an internal field E_o in the direction of the c-axis of the crystal, the circular damaging beam experiment was carried out. The spatial distribution of $\Delta(n_e-n_o)$ can be explained qualitatively using Chen's model. For this irradiation geometry, $\Delta(n_e-n_o)$ increases linearly with time up an an exposure time of 20 seconds which corresponds to an exposure energy density of 500J/cm^2. Based on King's analysis of optical damage in KTN, the problem for the circular damaging beam was solved using finite difference method. The resulting plot of $E_x(x,y)$ shows the same features as the experimental plot of $\Delta(n_e-n_o)$. No numerical comparison of experimental and theoretical results are possible since there are two unknowns, $\alpha\mu\tau$ and E_o, to be determined from one experiment.

To investigate the idea of an internal field, an experiment using

a narrow strip of light has been carried out. When the strip is perpendicular to the c-axis, drift would be the dominant mechanism affecting the movement of electrons. An analysis of this problem has been carried out based on Chen's model. Compared to King's analysis, no approximation as to the form of $n_o(x,y)$ is necessary. Numerical comparison between theory and experiment gave a value of 0.09 ± 0.005 cm for the product $\mu_n \tau E_o$. The case for the slit parallel to the c-axis where diffusion is the dominant mechanism has also been solved analytically. However, no experimental results have been obtained. This is not unexpected since the diffusion length of electrons is probably too small to be resolved with our present experimental set up.

From the above studies, it can be concluded that Chen's model is basically correct but the various parameters of the process need further investigation. Further work in this area involves the actual storage of holograms both on pure lithium niobate crystals and crystals doped with iron; the latter are useful as far as holographic storage is concerned since the writing time and the writing energy are less than the undoped crystals. As far as the engineering aspects of the process are concerned, future work should concentrate on improving the sensitivity to optical damage and the fixing of the holograms stored.

APPENDIX

Solution of 'Optical Damage' Problem for a Circular Laser Beam

Finite difference methods were used to solve the following equations which were explained in Chapter III.

$$\frac{\partial \rho}{\partial t} = - \nabla . \left[q \, n_o \mu \, (\vec{E}_o + \vec{E}) \right] \tag{1}$$

$$\vec{E}(x,y,t) = - \frac{1}{2\pi\epsilon_o\varepsilon} \nabla_{x,y} \left[\iint \rho(x',y',t) \, \ell n |\vec{r}| \, dx'dy' \right] \tag{2}$$

where

$$n_o(x,y) = \frac{2P_o\alpha\tau}{\pi h\nu r_o^2} \exp - \frac{2(x^2 + y^2)}{r_o^2} \tag{3}$$

The partial differential equations are approximated by finite difference equations through the transformation scheme below. The value of a variable z(x,y,t) are then determined at a discrete mesh of points in (x,y,t) space.

The partial derivative is approximated by

$$\frac{\partial \rho}{\partial t} = \frac{\rho(x_i,y_j,t_k+\Delta t) - \rho(x_i,y_j,t_k)}{\Delta t}$$

Let

$$\vec{A} = q \, n_o \, \mu(\vec{E}_o + \vec{E}) = A_x \, \hat{x} + A_y \, \hat{y}$$

$$c_1 = (q\mu) \frac{2P_o\alpha\tau}{\pi h\nu r_o^2}$$

$$A \exp = \exp \frac{2[((10-i)\Delta x)^2 + ((10-j)\Delta y)^2]}{r_o^2}$$

For an internal field $\vec{E}_o$ in the x direction only, that is

$$\vec{E}_o = E_o \hat{x}$$

we have

$$A_x = q\, n_o\, \mu(E_x + E_o)$$

$$A_y = q\, n_o\, \mu E_y$$

Hence

$$A_x(x_i,y_j,t_k) = C_1\, A \exp\,(x_i,y_j)\, [E_x(x_i,y_j,t_k) + E_o)$$

$$A_y(x_i,y_j,t_k) = C_1\, A \exp\,(x_i,y_j)\, [E_y(x_i,y_j,t_k)]$$

The indices i,j both run from 1 to 20 and hence there are 400 mesh points (figure 1).

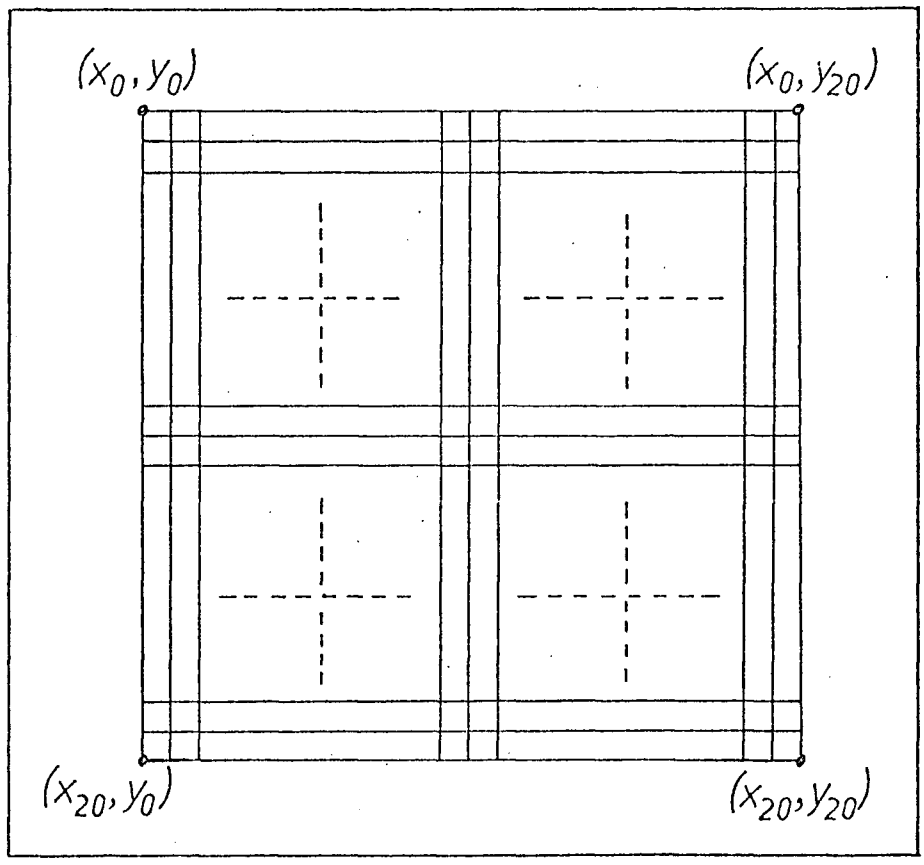

Figure 1: Square grid of mesh points used in the iteration scheme.

For any vector quantity $\vec{A} = A_x \hat{x} + A_y \hat{y}$

$$\nabla \cdot A = \frac{\partial A_x}{\partial x} + \frac{\partial A_y}{\partial y}$$

Hence Equation (1) becomes transformed into the following difference equation

$$\frac{\rho(x_i,y_j,t_k+\Delta t) - \rho(x_i,y_j,t_k)}{\Delta t}$$

$$= -\left\{ \frac{A_x(x_{i+1},y_j,t_k) - A_x(x_i,y_j,t_k)}{\Delta x} + \frac{A_y(x_i,y_{j+1},t_k) - A_y(x_i,y_j,t_k)}{\Delta y} \right\}$$

In the iteration scheme a square grid is used, that is,

$$\Delta x = \Delta y = h$$

Hence we have

$$\rho(x_i,y_j,t_k+\Delta t) = \rho(x_i,y_j,t_k) - \frac{\Delta t}{h} [A_x(x_{i+1},y_j,t_k) - A_x(x_i,y_j,t_k) + A_y(x_i,y_{j+1},t_k) - A_y(x_i,y_j,t_k)] \quad (4)$$

Equation (2) can be separated into two component equations as;

$$E_x(x,y,t) = -\frac{1}{2\rho\varepsilon_o\varepsilon} \frac{\partial}{\partial x} [\int\int \rho(x',y',t) \ln|\vec{r}| \, dx'dy'] \quad (5)$$

$$E_y(x,y,t) = -\frac{1}{2\pi\varepsilon_o\varepsilon} \frac{\partial}{\partial y} [\int\int \rho(x',y',t) \ln|\vec{r}| \, dx'dy'] \quad (6)$$

Now

$$\frac{\partial}{\partial x} \ln|\vec{r}| = \frac{\partial}{\partial x} \ln (x-x')^2 + (y-y')^2 = \frac{(x-x')}{(x-x')^2+(y-y')^2}$$

Similarly,

$$\frac{\partial}{\partial y} \ln|\vec{r}| = \frac{(y-y')}{(x-x')^2+(y-y')^2}$$

Equations (5) and (6) therefore becomes

$$E_x(x_i,y_j,t_k) = -\frac{1}{2\pi\,\varepsilon_o\varepsilon}\left[\iint\rho(x',y',t_k)\,\frac{(x_i-x')}{(x_i-x')^2+(y_j-y')^2}\,dx'dy'\right] \quad (7)$$

$$E_y(x_i,y_j,t_k) = -\frac{1}{2\pi\varepsilon_o\varepsilon}\left[\iint\rho(x',y',t_k)\,\frac{(y_j-y')}{(x_i-x')^2+(y_j-y')^2}\,dx'dy'\right] \quad (8)$$

The numerical integrations are carried out using Trapezoidal Rule of Integration (Figure 2)

$$\int_{x_o}^{x_n} y(x)\,dx = \frac{h}{2}\left[y_o + 2y_1 + 2y_2 + \ldots + 2y_{n-1} + y_n\right]$$

$$= h\left[\frac{(y_o+y_n)}{2} + (y_1 + y_2 + \ldots + y_{n-1})\right]$$

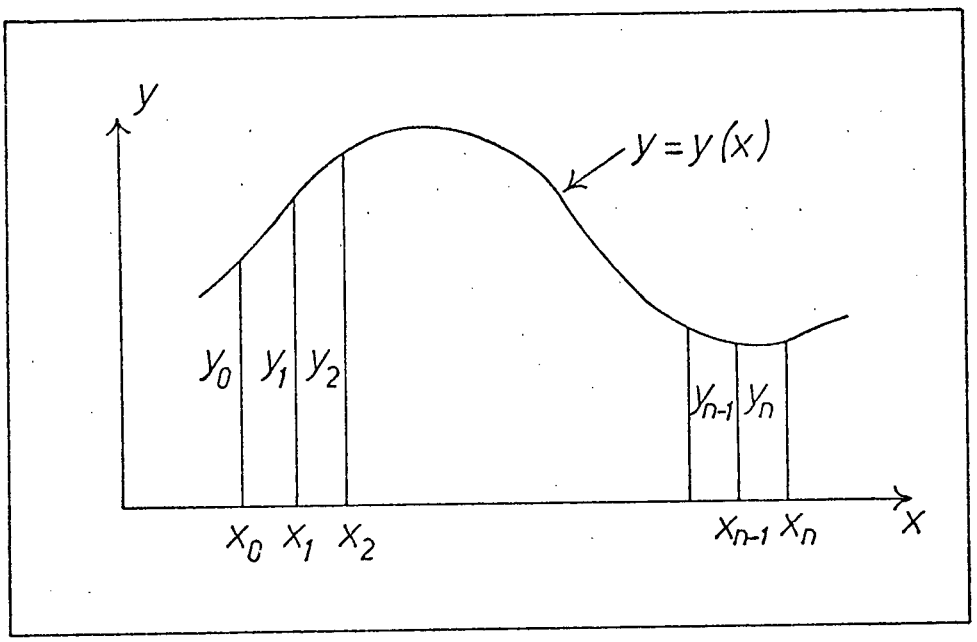

Figure 2: Trapezoidal rule of integration given y = y(x).

Let

$$B(x',y',x_i,y_j) = \rho(x',y',t_k) \frac{(x_i - x')}{(x_i-x')^2+(y_j-y')^2}$$

Equation (7) becomes

$$\iint \rho(x',y',t_k) \frac{(x_i-x')}{(x_i-x')^2+(y_j-y')^2} \, dx'dy'$$

$$= \iint B(x',y',x_i,y_j) \, dx'dy' = \iint dy' \int B(x',y',x_i,y_j) \, dx'$$

$$= \int dy' \left[\sum_{\ell} \Delta x \, [B(x', y_n', x_i,y_j)] + \right.$$

$$\left. \frac{\Delta x}{2} [B(x_1',y_n',x_i,y_j) + B(x_{20}',y_n',x_i,y_j)] \right]$$

The integration with respect to y' is then similarly carried out and equation (8) is similarly solved.

The initial conditions for the iteration scheme are

$$E_x (x_i,y_j,t_k=0) = 0$$

$$E_y (x_i,y_j,t_k=0) = 0$$

$$\rho(x_i,y_j,t_k=0) = 0$$

$$E_o = \text{constant}$$

A copy of the Fortran program based on the above iteration scheme is appended. The program evaluates $\rho(x,y,t)$, $E_x(x,y,t)$ and $E_y(x,y,t)$ at a discrete mesh of points (x,y) for a specified number of iterations. ρ, E_x and E_y are then plotted out as a perspective drawing using the program UBC PERSP in the UBC Computing Centre File.

```
FORTRAN IV G COMPILER        MAIN            12-01-72        01:24:55        PAGE 0001

0001                 DIMENSION EX(21,21),EY(21,21),AX(21,21),AY(21,21),RHO(21,21),
                    CAEXP(20,20),B(20,20),C(20,20),X(20,20),Y(20,20),Z(20,20)
0002                 REAL PO
0003                 INTEGER P,Q,R
0004                 WRITE (6,2)
0005               2 FORMAT (1H1, 83HCALCULATION OF THE SPACE CHARGE FIELD IN LITHIUM N
                    CIOBATE WHEN EXPOSED TO LASER BEAM)
                   C READ IN INITIAL VALUES FOR VARIOUS PARAMETERS
                   C ANT=PRODUCT OF
                   C PO=POWER OF THE LASER BEAM
                   C FREQ=FREQUENCY OF THE LASER BEAM
                   C RO=RADIUS OF THE LASER BEAM
                   C H=SIZE OF THE GRID SQUARE IN METRES
                   C EO=VALUE OF THE INTERNAL ELECTRIC FIELD IN VOLTS/M
                   C DELT=INCREMENT OF THE TIME OF ITERATION
                   C EPSIL=PERMITTIVITY OF THE LITHIUM NIOBATE
0006                 READ (5,1) ANT,PO,FREQ,H,RO,EO,DELT,EPSIL,Q
0007               1 FORMAT (8E3.3,I2)
0008                 WRITE (6,902) ANT,PO,FREQ,H,RO,EO,DELT,EPSIL,Q
0009             902 FORMAT (1HO, 8(E9.3,3X),I2)
0010                 C1=(2.0*PO*(1.6E-19)*ANT)/(3.14159*(6.625E-34))
0011                 C2=(-1.0)/(2.0*3.14159*EPSIL)
0012                 WRITE (6,609) C1,C2
0013             609 FORMAT (1HO, E10.3,E10.3)
                   C INITIALISE THE VARIOUS ARRAYS
0014                 P=1
0015                 R=0
0016                 DO 10 I=1,21
0017                 DO 10 J=1,21
0018                 EX(I,J)=0.0
0019                 EY(I,J)=0.0
0020                 AX(I,J)=0.0
0021                 AY(I,J)=0.0
0022              10 RHO(I,J)=0.0
                   C START CALCULATION OF RHO
0023                 DO 20 I=1,20
0024                 DO 20 J=1,20
0025              20 AEXP(I,J)=EXP(-2.0*((((10-I)**2)+((10-J)**2))/(RO*RO))*H*H)
0026              40 DO 50 I=1,20
0027                 DO 50 J=1,20
0028                 AX(I,J)=AEXP(I,J)*(EX(I,J)+EO)
0029              50 AY(I,J)=AEXP(I,J)*EY(I,J)
0030                 DO 60 J=1,20
0031                 AX(21,J)=AX(19,J)
0032              60 AY(J,21)=AY(J,19)
0033                 DO 65 I=1,20
0034                 DO 65 J=1,20
0035              65 RHO(I,J)=RHO(I,J)-C1*(((AX(I+1,J)-AX(I,J))+(AY(I,J+1)-AY(I,J)))/H)
                    C*DELT
0036                 WRITE (6,3) P
0037               3 FORMAT (1HO, 20HNO. OF ITERATIONS=  ,I2)
                   C EVALUATION OF EX AND EY USING ITERATIVE FORMULA
0038                 I=0
0039             900 I=I+1
0040                 WRITE (6,962) I
```

```
FORTRAN IV G COMPILER        MAIN            12-01-72        01:24:55        PAGE 0002

0041          962  FORMAT (1HO, 4HI=  ,I2)
0042               IF (I .EQ. 21) GO TO 600
0043               J=0
0044          500  J=J+1
0045               DO 70 L=1,20
0046               DO 70 M=1,20
0047               IF (I .EQ. L .AND. J .EQ. M) GO TO 71
0048               C4=RHO(L,M)/(((I-L)**2+(J-M)**2)*H)
0049               B(L,M)=C4*(I-L)
0050               C(L,M)=C4*(J-M)
0051               GO TO 70
0052           71  B(L,M)=0.0
0053               C(L,M)=0.0
0054           70  CONTINUE
                 C INITIALISE THE TEMPORARY PARAMETERS
0055               BTEMP1=0.0
0056               BTEMP2=0.0
0057               BTEMP3=0.0
0058               BTEMP4=0.0
0059               BTEMP5=0.0
0060               CTEMP1=0.0
0061               CTEMP2=0.0
0062               CTEMP3=0.0
0063               CTEMP4=0.0
0064               CTEMP5=0.0
0065               DO 80 L=2,19
0066               DO 80 M=2,19
0067               BTEMP1=BTEMP1+B(L,M)
0068           80  CTEMP1=CTEMP1+C(L,M)
0069               DO 90 N=2,19
0070               BTEMP2=BTEMP2+B(N,1)
0071               BTEMP3=BTEMP3+B(N,20)
0072               BTEMP4=BTEMP4+B(1,N)
0073               BTEMP5=BTEMP5+B(20,N)
0074               CTEMP2=CTEMP2+C(N,1)
0075               CTEMP3=CTEMP3+C(N,20)
0076               CTEMP4=CTEMP4+C(1,N)
0077           90  CTEMP5=CTEMP5+C(20,N)
0078               EX(I,J)=C2*H*H*(BTEMP1+0.5*(BTEMP2+BTEMP3+BTEMP4+BTEMP5)+0.25*(B(1
                 C,1)+B(1,20)+B(20,1)+B(20,20)))
0079          100  EY(I,J)=C2*H*H*(CTEMP1+0.5*(CTEMP2+CTEMP3+CTEMP4+CTEMP5)+0.25*(C(1
                    C,1)+C(1,20)+C(20,1)+C(20,20)))
0080               IF (J .EQ. 20) GO TO 900
0081               GO TO 500
0082          600  R=R+1
0083               IF (R .EQ. 9) GO TO 601
0084               GO TO 449
0085          601  DO 534 I=1,20
0086               WRITE (6,533) (RHO(I,J), J=1,20)
0087          533  FORMAT (1HO, 10(E10.3,2X)/10(E10.3,2X))
0088           534 CONTINUE
0089               DO 543 I=1,20
0090               WRITE (6,544) (EX(I,J),J=1,20)
0091          544  FORMAT (1HO, 10(E10.3,2X)/10(E10.3,2X))
0092          543  CONTINUE
```

```
FORTRAN IV G COMPILER        MAIN            12-01-72        01:24:55        PAGE 0003

0093                 DO 553 I=1,20
0094                 WRITE (6,555) (EY(I,J),J=1,20)
0095           555   FORMAT (1H0, 10(E10.3,2X)/10(E10.3,2X))
0096           553   CONTINUE
0097                 DO 883 I=1,20
0098                 DO 883 J=1,20
0099           883   Z(I,J)=RHO(I,J)
0100                 DO 931 I=1,20
0101                 DO 931 J=1,20
0102           931   Y(I,J)=EX(I,J)
0103                 DO 217 I=1,20
0104                 DO 217 J=1,20
0105           217   X(I,J)=EY(I,J)
0106                 CALL PERS (Z,20,20,20,1.0,0.6,10.0,45.0,10.0,10.0)
0107                 CALL PLOT (20.0,0.0,-3)
0108                 CALL PERS (Y,20,20,20,1.0,0.6,10.0,45.0,10.0,10.0)
0109                 CALL PLOT(20.0,0.0,-3)
0110                 CALL PERS (X,20,20,20,1.0,0.6,10.0,45.0,10.0,10.0)
0111                 CALL PLOTND
0112            449  P=P+1
0113                 IF (P .EQ. 10) GO TO 987
0114                 GO TO 40
0115           987   STOP
0116                 END

 TOTAL MEMORY REQUIREMENTS 0057BE BYTES

 COMPILE TIME =       5.7  SECONDS
```

REFERENCES

1. W.C. Stewart, R.S. Mezrich, L.S. Cosentino, E.M. Nagle, F.S. Wendt and R.D. Lohman, RCA Review, 34, 3 (1973).

2. W. Phillips, J.J. Amodei and D.L. Staebler, RCA Review, 33, 94 (1972).

3. J.J. Amodei and D.L. Staebler, RCA Review, 32, 71 (1971).

4. D.L. Staebler and J.J. Amodei, Ferroelectrics, 3, 107 (1972).

5. A. Ashkin, G.D. Boyd, J.M. Dziedzic, R.G. Smith, A.A. Ballman, J.J. Levinstein and K. Nassau, Appl. Phys. Letters, 9, 72 (1966).

6. F.S. Chen, J.T. LaMacchia and D.B. Fraser, Appl. Phys. Letters, 13, 223 (1968).

7. T.K. Gaylord, T.A. Rabson and F.K. Tittel, Appl. Phys. Letters, 20, 47 (1972).

8. S.R. King, T.S. Hartwick and A.B. Chase, Appl. Phys. Letters, 21, 312 (1972).

9. G.D. Boyd, W.L. Bond and H.L. Carter, J. Appl. Phys., 38, 1941 (1967).

10. F.S. Chen, J. Appl. Phys., 40, 3389 (1969).

11. W.D. Johnston, Jr., J. Appl. Phys., 41, 3279 (1970).

12. J.J. Amodei, RCA Review, 32, 185 (1971).

13. J.F. Nye, Physical Properties of Crystals (Oxford University Press, Oxford, 1960).

14. J.E. Midwinter, Appl. Phys. Letters, 11, 128 (1967).